

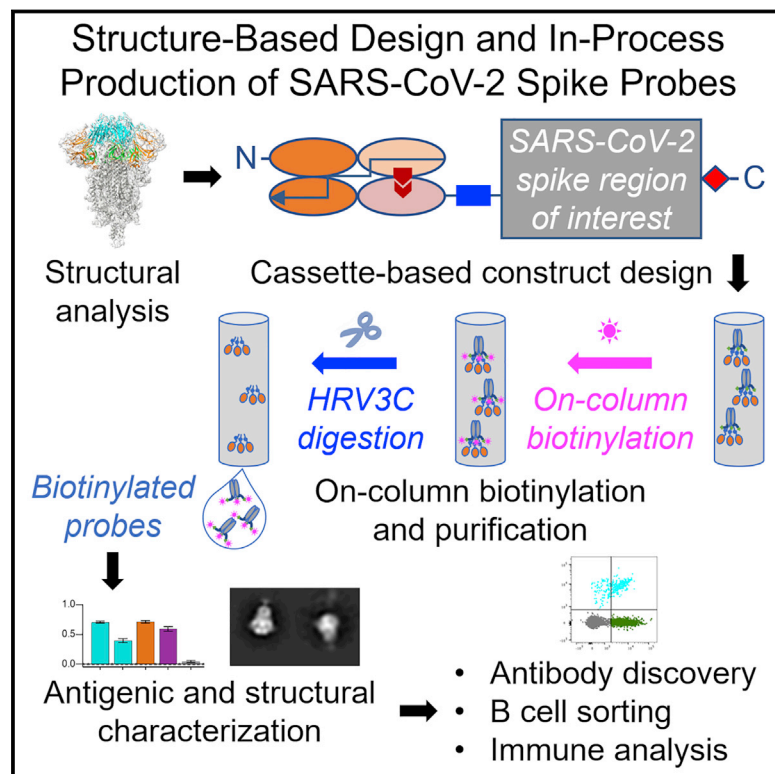


Since January 2020 Elsevier has created a COVID-19 resource centre with free information in English and Mandarin on the novel coronavirus COVID-19. The COVID-19 resource centre is hosted on Elsevier Connect, the company's public news and information website.

Elsevier hereby grants permission to make all its COVID-19-related research that is available on the COVID-19 resource centre - including this research content - immediately available in PubMed Central and other publicly funded repositories, such as the WHO COVID database with rights for unrestricted research re-use and analyses in any form or by any means with acknowledgement of the original source. These permissions are granted for free by Elsevier for as long as the COVID-19 resource centre remains active.

Structure-Based Design with Tag-Based Purification and In-Process Biotinylation Enable Streamlined Development of SARS-CoV-2 Spike Molecular Probes

Graphical Abstract



Authors

Tongqing Zhou, I-Ting Teng, Adam S. Olia, ..., Nancy J. Sullivan, Lawrence Shapiro, Peter D. Kwong

Correspondence

Iss8@columbia.edu (L.S.),
pdkwong@nih.gov (P.D.K.)

In Brief

SARS-CoV-2 spike probes are key to antibody discovery and vaccine evaluation. By using structure-based design, affinity purification, on-column biotinylation, and sequence-specific protease cleavage, Zhou et al. devise a strategy that allows for the rapid development of SARS-CoV-2 spike probes for B cell sorting, antibody discovery, and immune assessment.

Highlights

- Structure-based design of SARS-CoV-2 spike ectodomain and subdomain probes
- On-column biotinylation and purification is enabled by affinity tag and HRV3C cleavage
- Development of diverse molecular probes by “cut-and-paste” strategy
- Application of probes to SARS-CoV-2 antibody discovery and immune evaluation



Article

Structure-Based Design with Tag-Based Purification and In-Process Biotinylation Enable Streamlined Development of SARS-CoV-2 Spike Molecular Probes

Tongqing Zhou,¹ I-Ting Teng,^{1,8} Adam S. Olia,^{1,8} Gabriele Cerutti,^{2,8} Jason Gorman,^{1,8} Alexandra Nazzari,^{1,8} Wei Shi,¹ Yaroslav Tsybovsky,³ Lingshu Wang,¹ Shuishu Wang,¹ Baoshan Zhang,¹ Yi Zhang,¹ Phinikoula S. Katsamba,² Yuliya Petrova,¹ Bailey B. Banach,⁴ Ahmed S. Fahad,⁵ Lihong Liu,⁶ Sheila N. Lopez Acevedo,⁵ Bharat Madan,⁵ Matheus Oliveira de Souza,⁵ Xiaoli Pan,⁵ Pengfei Wang,⁶ Jacy R. Wolfe,⁵ Michael Yin,⁶ David D. Ho,⁶ Emily Phung,¹ Anthony DiPiazza,¹ Lauren A. Chang,¹ Olubukola M. Abiona,¹ Kizzmekia S. Corbett,¹ Brandon J. DeKosky,^{4,5,7} Barney S. Graham,¹ John R. Mascola,¹ John Misasi,¹ Tracy Ruckwardt,¹ Nancy J. Sullivan,¹ Lawrence Shapiro,^{1,2,*} and Peter D. Kwong^{1,2,9,*}

¹Vaccine Research Center, National Institute of Allergy and Infectious Diseases, National Institutes of Health, Bethesda, MD 20892, USA

²Department of Biochemistry and Molecular Biophysics, Columbia University, New York, NY 10032, USA

³Electron Microscopy Laboratory, Cancer Research Technology Program, Leidos Biomedical Research Inc., Frederick National Laboratory for Cancer Research, Frederick, MD 21701, USA

⁴Bioengineering Graduate Program, The University of Kansas, Lawrence, KS 66045, USA

⁵Department of Pharmaceutical Chemistry, The University of Kansas, Lawrence, KS 66045, USA

⁶Aaron Diamond AIDS Research Center, Columbia University Vagelos College of Physicians and Surgeons, New York, NY 10032, USA

⁷Department of Chemical Engineering, The University of Kansas, Lawrence, KS 66045, USA

⁸These authors contributed equally

⁹Lead Contact

*Correspondence: iss8@columbia.edu (L.S.), pdkwong@nih.gov (P.D.K.)

<https://doi.org/10.1016/j.celrep.2020.108322>

SUMMARY

Biotin-labeled molecular probes, comprising specific regions of the severe acute respiratory syndrome coronavirus 2 (SARS-CoV-2) spike, would be helpful in the isolation and characterization of antibodies targeting this recently emerged pathogen. Here, we design constructs incorporating an N-terminal purification tag, a site-specific protease-cleavage site, the probe region of interest, and a C-terminal sequence targeted by biotin ligase. Probe regions include full-length spike ectodomain as well as various subregions, and we also design mutants that eliminate recognition of the angiotensin-converting enzyme 2 (ACE2) receptor. Yields of biotin-labeled probes from transient transfection range from ~0.5 mg/L for the complete ectodomain to >5 mg/L for several subregions. Probes are characterized for antigenicity and ACE2 recognition, and the structure of the spike ectodomain probe is determined by cryoelectron microscopy. We also characterize antibody-binding specificities and cell-sorting capabilities of the biotinylated probes. Altogether, structure-based design coupled to efficient purification and biotinylation processes can thus enable streamlined development of SARS-CoV-2 spike ectodomain probes.

INTRODUCTION

Severe acute respiratory syndrome coronavirus 2 (SARS-CoV-2), the causative agent for coronavirus disease 2019 (COVID-19), emerged in 2019 and rapidly spread, infecting millions, overwhelming healthcare systems, and impacting economies worldwide (Callaway et al., 2020; Cucinotta and Vanelli, 2020). To respond, a global effort has been initiated to develop vaccines and therapeutic agents. For COVID-19 vaccine development (reviewed in Callaway, 2020), the trimeric SARS-CoV-2 spike—a type 1 fusion machine that facilitates virus cell entry through interaction with the angiotensin-converting enzyme 2 (ACE2) receptor (Hoffmann et al., 2020; Ou et al., 2020)—is a lead target, as antibodies against it can block virus entry (Jiang et al., 2020). Most

of the SARS-CoV-2-neutralizing antibodies so far isolated target the receptor binding domain (RBD) of the spike protein (Brouwer et al., 2020; Cao et al., 2020; Chen et al., 2020; Chi et al., 2020; Ju et al., 2020; Liu et al., 2020b; Pinto et al., 2020; Robbiani et al., 2020; Rogers et al., 2020; Seydoux et al., 2020; Wang et al., 2020a; Wrapp et al., 2020a; Wu et al., 2020; Zeng et al., 2020; Zost et al., 2020), but there are other sites in the N-terminal domain (NTD) and S2 stem domain that have also been associated with neutralizing activity against other betacoronaviruses (Pallesen et al., 2017; Wang et al., 2018b). Such virus-neutralizing antibodies are sought as therapeutic and prophylactic agents (Cao et al., 2020; reviewed in Graham et al., 2013; Zhou and Zhao, 2020).

Biotin-labeled molecular probes, comprising the SARS-CoV-2 spike as well as its discrete domains, can accelerate



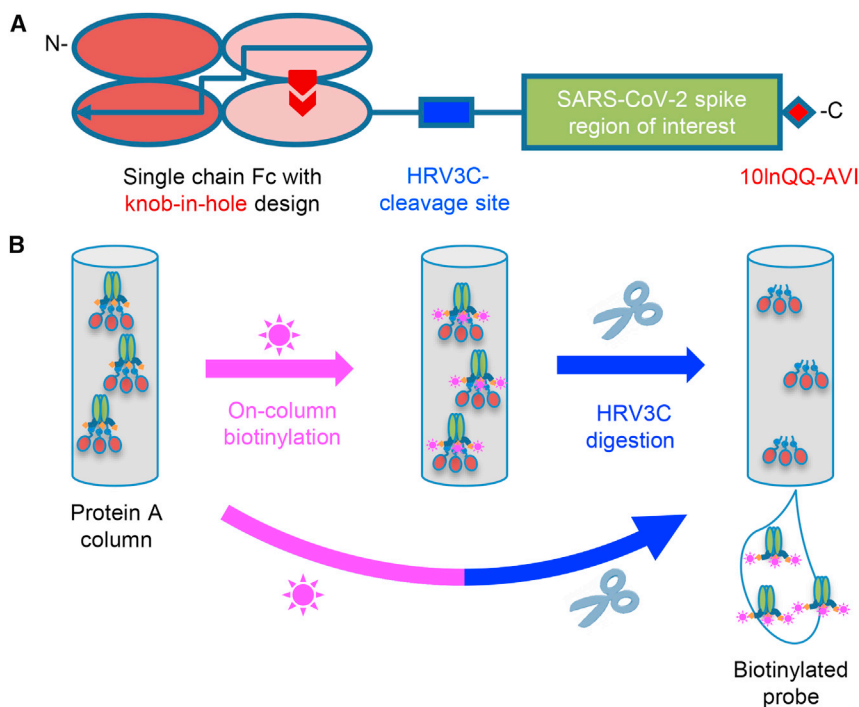


Figure 1. Strategy for Tag-Based Purification with On-Column Biotinylation

(A) Schematic design of the expression construct of SARS-CoV-2 molecular probes. A single-chain human Ig constant domain (scFc) was added at the N terminus to facilitate expression and purification. The AVI tag was placed at the C terminus after a 10-amino-acid linker for biotinylation. The red arrows in the second and fourth Fc domains showed the “knob-in-hole” mutations to prevent dimerization of the scFc.

(B) Biotinylation and HRV3C digestion. Cell culture supernatant from cells transiently transfected with plasmid was loaded onto protein A affinity column. Biotinylation and HRV3C cleavage reactions can be carried out in series or simultaneously, as buffers for both reactions are compatible.

RESULTS

Strategy for Tag-Based Purification with In-Process Biotinylation

To facilitate purification and biotinylation, we devised a probe construct using the constant portion of an antibody (Fc) as an N-terminal purification tag. Fc expresses

and folds efficiently and can be effectively captured by protein A resins (Jäger et al., 2013). To prevent intermolecular dimer formation of the Fc tag, we used a single-chain human Ig constant domain (scFc) with “knob-in-hole” feature (Ridgway et al., 1996), in which a “knob” comprising a protruding Tyr (T366Y) was incorporated into the N-terminal half of the Fc-interface, followed by a 20-residue linker (GGGGS)₄, and a “hole” comprising a recessed threonine (Y407T) was incorporated into the C-terminal-half of the Fc-interface (Kabat antibody residue numbering; Johnson and Wu, 2000) (Figure 1A).

development of both vaccines and therapeutic antibodies. For vaccine development, such probes can be used to track humoral responses longitudinally (Liu et al., 2011; Yongchen et al., 2020) and to quantify elicited responses against the spike and its domains, as correlating such responses with neutralization should provide crucial insight into sites of spike vulnerability. For antibody identification, probes are used in B cell sorting to identify B cells encoding antibodies capable of recognizing the spike or particular spike domains as well as characterizing antibody binding affinities through surface plasmon resonance (SPR) or bio-layer interferometry (BLI) analyses.

Here, we describe the structure-based design of molecular probes, encompassing the SARS-CoV-2 spike and its domains. We first designed a construct that allowed for tag-based purification and on-column biotinylation. Next, we incorporated the SARS-CoV-2 spike ectodomain, with prefusion-stabilizing mutations and a C-terminal trimerization motif, which we expressed, biotinylated, purified, and characterized, including by cryoelectron microscopy (cryo-EM). Based on the structure-defined spike-domain organization (Walls et al., 2020; Wrapp et al., 2020b), we also created and characterized separate molecular probes comprising the NTD, the RBD, and RBD with spike domain 1 (RBD-SD1). We also used the structural information of RBD interactions with ACE2 (Lan et al., 2020; Wang et al., 2020b; Yan et al., 2020a) to define mutations that could inhibit ACE2 interaction, which we incorporated into mutant RBD probes with ACE2 recognition ablated. Finally, we characterized properties of the devised probes including degree of biotinylation, antibody-binding specificity, and use in sorting yeast cells expressing SARS-CoV-2 spike-binding antibodies or B cells from a COVID-19 convalescent donor. Overall, our findings demonstrate how structure-based design can be used to develop molecular probes of the SARS-CoV-2 spike.

and folds efficiently and can be effectively captured by protein A resins (Jäger et al., 2013). To prevent intermolecular dimer formation of the Fc tag, we used a single-chain human Ig constant domain (scFc) with “knob-in-hole” feature (Ridgway et al., 1996), in which a “knob” comprising a protruding Tyr (T366Y) was incorporated into the N-terminal half of the Fc-interface, followed by a 20-residue linker (GGGGS)₄, and a “hole” comprising a recessed threonine (Y407T) was incorporated into the C-terminal-half of the Fc-interface (Kabat antibody residue numbering; Johnson and Wu, 2000) (Figure 1A).

Between the scFc and the target region of interest (Figure 1A), we added a cleavage site for the human rhinovirus 3C (HRV3C) protease (Cordingley et al., 1990), a highly specific protease that recognizes the sequence LEVLFGQP, cleaving after Q and leaving a GP dipeptide at the start of the target. This allowed us to remove the target protein from the protein A-capture resin by protease treatment, avoiding low pH elution that is known to alter the conformations of type 1 fusion machine and could potentially alter the conformation of the probe. After the target sequence of interest, we incorporated a 10-residue linker followed by a biotin ligase-specific sequence (10InQQ-AVI). This construct design enabled capture by protein A and on-column biotinylation (Figure 1B). As buffers for biotinylation and HRV3C cleavage are compatible, the entire process of biotinylation, HRV3C cleavage, and purification could in principle be accomplished with a single column, although we have generally added a polishing size-exclusion chromatography step to ensure size homogeneity.

Molecular Probe of Stabilized SARS-CoV-2 Spike Trimer with Biotinylation

To obtain a molecular probe of the SARS-CoV-2 spike, we incorporated stabilizing mutations into the spike target protein

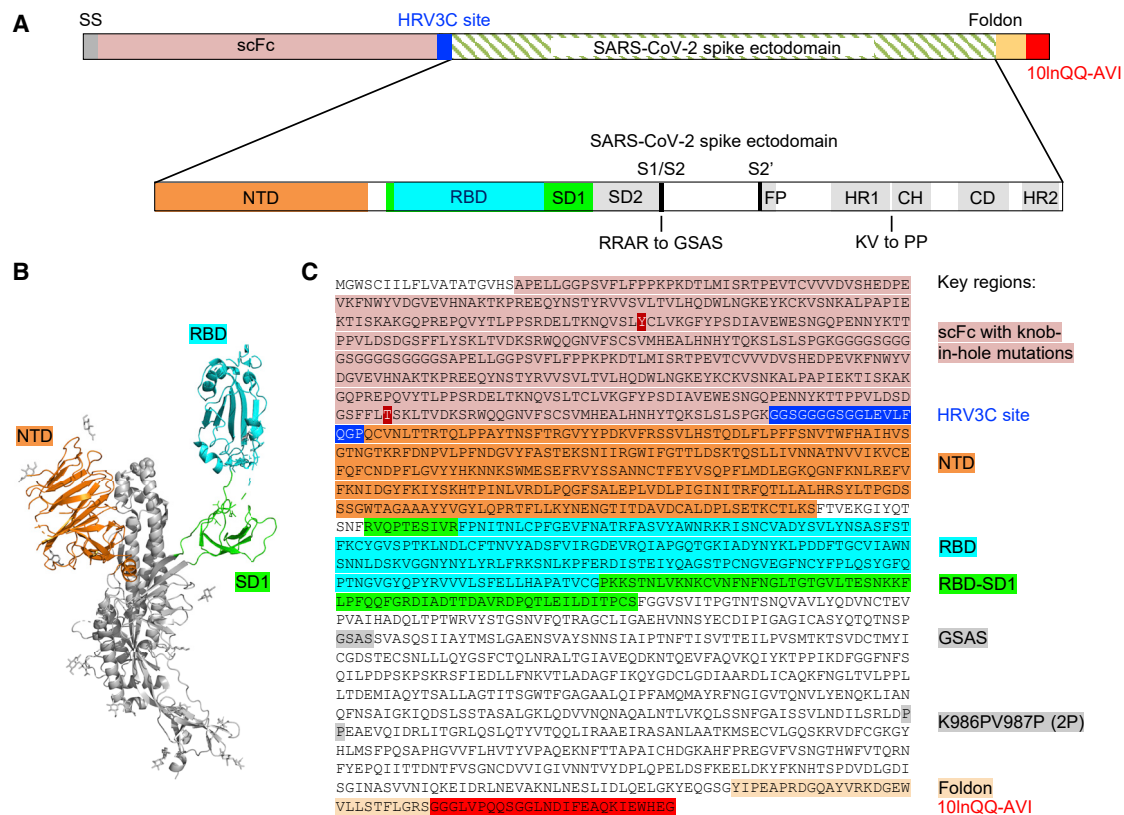


Figure 2. Design of the SARS-CoV-2 Spike S2P Molecular Probe

(A) Schematic of construction of the SARS-CoV-2 spike probe containing the ectodomain of the spike protein, the GSAS mutations replacing the RRAR furin cleavage site, and the K986PV987P (2P) mutation stabilizing the spike in pre-fusion conformation, a foldon domain, and a 10-amino-acid linker (10InQQ), followed by the AVI tag.

(B) Structural model of a SARS-CoV-2 spike protomer with the NTD, RBD, and SD1 domains highlighted.

(C) Sequence of the SARS-CoV-2 spike probe with key regions annotated.

See also [Table S1](#).

residues 14 to 1208 (Wrapp et al., 2020b), replacing amino acids RRAR at the S1/S2 cleavage site with GSAS and KV between domains HR1 and CH with PP (Figure 2; Table S1) and adding the T4-phage fibrin trimerization domain (foldon) at the C terminus (Efimov et al., 1994; Miroshnikov et al., 1998) (this construct is hereafter referred to as S2P), and expressed it by transient mammalian cell transfection. We observed cleavage by HRV3C protease to be impeded with the glutathione S-transferase-tagged, but not the His-tagged, version of the protease, suggesting partial steric constraints on access to the HRV3C site; overall, we could obtain ~0.5 mg of the purified S2P probe per liter of cell culture after 24 h of incubation at 4°C with the His-tagged HRV3C.

The protease-liberated probe SARS-CoV-2 S2P ran primarily as a single peak on size-exclusion chromatography and a major band on SDS-PAGE (Figures 3A and 3B), appeared homogeneous by negative-stain EM (Figure 3C), and was recognized by the RBD-binding antibody CR3022 (Tian et al., 2020; Yuan et al., 2020). We characterized binding to three antibodies from a SARS-CoV convalescent donor S652: S652-109, which recognizes the RBD; S652-112, which recognizes an epitope in S2;

and S652-118, which recognizes the NTD. The S2P probe bound to all three of these antibodies, as well as the ACE2 receptor, but not to soluble CD4 (D1D2-sCD4) or antibody VRC01 (Wu et al., 2010), which bound a control probe encompassing HIV-1 envelope glycoprotein (Env) trimer BG505 DS-SOSIP (Figure 3D). We further characterized binding to four antibodies recently isolated from SARS-CoV-2 convalescent donors: antibodies 2-4 (Liu et al., 2020a) and B38 (Wu et al., 2020), which recognize the RBD; 4-8 (Liu et al., 2020a), which recognizes the NTD; and 2-51 (Liu et al., 2020a), which clusters with other NTD-directed antibodies. All of these antibodies showed positive binding to the S2P probe (Figure 3D). Overall, these properties suggested the SARS-CoV-2 S2P probe to be a good biological mimic of the prefusion SARS-CoV-2 spike ectodomain.

Cryo-EM Structure of a Biotinylated SARS-CoV-2 Spike Probe

To provide atomic-level insight into the mimicry of spike by probe, we determined the cryo-EM structure of the biotinylated SARS-CoV-2 S2P probe (Figures 3E and S3; Table S2). The cryo-EM grids were frozen with the biotinylated SARS-CoV-2

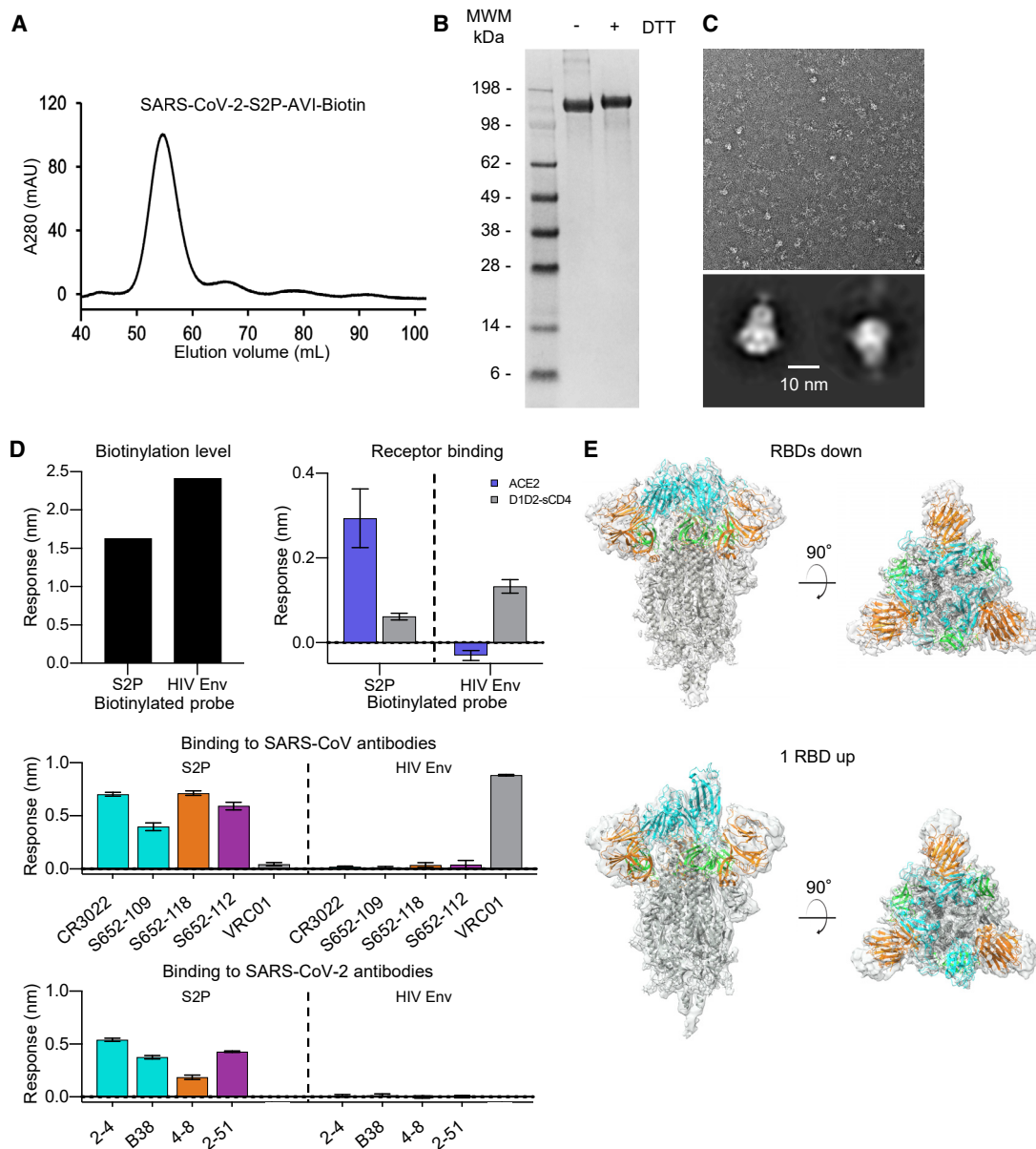


Figure 3. Physical Properties, Antigenic Characteristics, and Cryo-EM Structure of a Biotinylated SARS-CoV-2 S2P Probe

(A) Size-exclusion chromatography of the biotinylated SARS-CoV-2 S2P probe in PBS buffer.

(B) SDS-PAGE of the SARS-CoV-2 S2P probe with and without the reducing agent DTT. Molecular weight marker (MWM) was run alongside the probe.

(C) Negative-stain EM of the SARS-CoV-2 S2P probe. The 2D-class averages were shown below the wide-field raw EM image in 5-fold magnification. Scale bar: 10 nm.

(D) Biotinylation, receptor recognition, and antigenicity of the SARS-CoV-2 S2P probe. The level of biotinylation was evaluated by capture of probes at 40 $\mu\text{g}/\text{mL}$ onto the streptavidin biosensors. A biotinylated HIV-1 Env containing the same 10InQQ-AVI tag at the C terminus was used for comparison (top left). Binding to the ACE2 receptor (top right) and binding to SARS-CoV (middle) and SARS-CoV-2 (bottom) antibodies were assessed using 80 $\mu\text{g}/\text{mL}$ S2P or 20 $\mu\text{g}/\text{mL}$ HIV Env probes, respectively. Receptors and antibodies were set at 500 nM. Error bars represent standard deviation of triplicate measurements. HIV-1 receptor CD4 and antibody VRC01 were used as controls.

(E) Cryo-EM structures of biotinylated SARS-CoV-2 S2P probe. Domains are colored as in Figure 2C sequence. The C-terminal residues 1153-1208 plus the foldon, 10InQQ-AVI tag, and biotin were not visible in the electron density.

See also Figures S2 and S3 and Table S2.

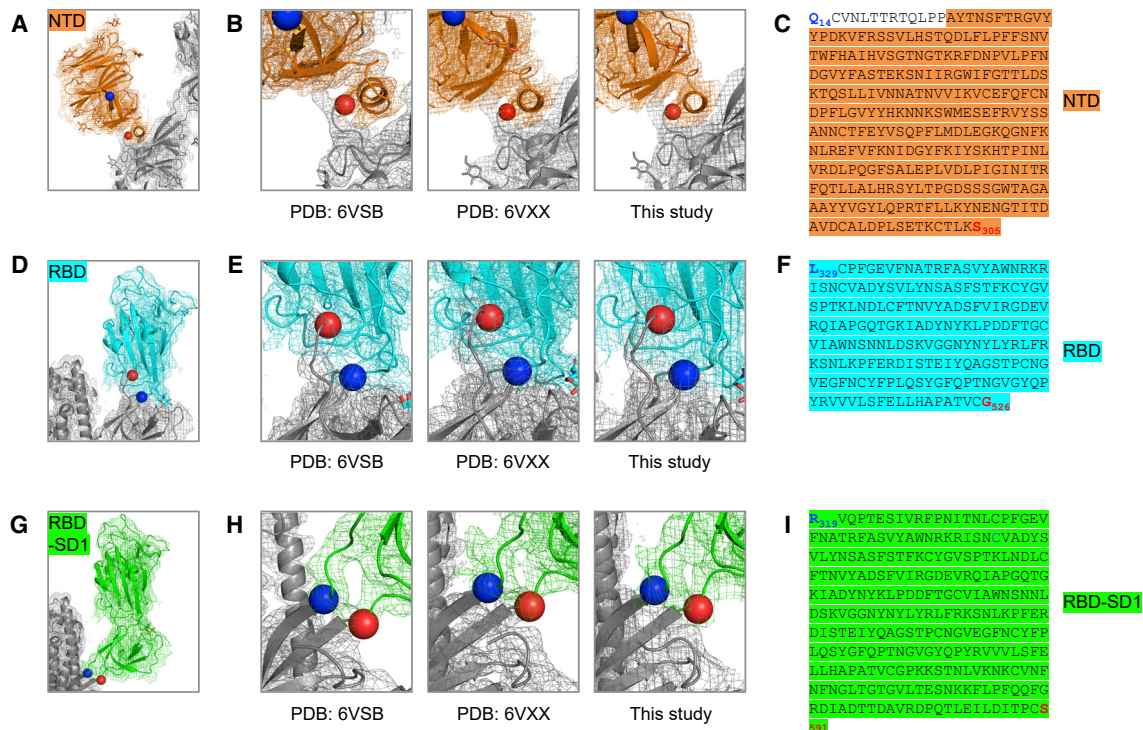


Figure 4. Structure-Based Definition of SARS-CoV-2 Molecular Probes Comprising the NTD, RBD, and RBD-SD1 Domains

(A) Cryo-EM structure of the NTD domain in the S2P probe determined in this study (Figure 3E), with reconstruction density shown in orange for NTD domain and in gray otherwise. First ordered residue with density (A27) is highlighted with a blue sphere; last residue of NTD domain (S305) is highlighted with a red sphere.
 (B) Close-up view of the NTD termini.
 (C) Sequence of NTD domain probe. The sequence is highlighted in orange except for residues 14–26, which are disordered in the cryo-EM structures.
 (D) Cryo-EM structure of the RBD domain in spike (Figure 3E), with reconstruction density shown in cyan for RBD domain and in gray otherwise. First residue with density (L329) is highlighted with a blue sphere; last ordered residue of RBD domain (G526) is highlighted with a red sphere.
 (E) Close-up view of the spike RBD termini.
 (F) Sequence of RBD domain probe highlighted in cyan.
 (G) Cryo-EM structure of the RBD-SD1 domains in spike (Figure 3E), with reconstruction density shown in green for RBD-SD1 domain and in gray otherwise. First residue with density (R319) is highlighted with a blue sphere; last ordered residue of RBD-SD1 domain (S591) is highlighted with a red sphere.
 (H) Close-up view of the spike RBD-SD1 termini.
 (I) Sequence of the RBD-SD1 domain probe highlighted in green.
 See also Figures S1 and S3 and Tables S1 and S2.

S2P probe in PBS at pH 7.4. We observed two distinct conformations: one with all three RBDs in the “down” position, displaying C3 symmetry; and the other with one RBD in the “up” position and the other two RBDs in the “down” position, C1 symmetric. We observed more particles (43,176) in the RBDs down conformation, which contributed to a 3.45-Å resolution map, whereas the single-RBD-up state (34,223 particles) 3D reconstruction achieved an overall resolution of 4.00 Å. The two final atomic models were very similar to published cryo-EM spike-ectodomain structures (Walls et al., 2020; Wrapp et al., 2020b). The C1-symmetric structure included residues 27–1147, while residues 27–1152 were modeled for the C3-symmetric structure; in both cases, some regions could not be modeled because of their intrinsic flexibility. Five additional residues at the C-terminal region (1148–1152) were visible in the reconstruction density of the RBDs down structure, but—similar to published structures (Walls et al., 2020; Wrapp et al., 2020b)—the C-terminal region of the S2 domain (and in our case the rest

of the probe) was not sufficiently ordered to be modeled. The two structures were similar except for the single RBD that was in the “up” position in the C1-symmetric structure. Excluding this single RBD, the root-mean-square deviation (RMSD) was 0.95 Å between the two probe structures for 2738 aligned C α atoms.

Molecular Probes Comprising SARS-CoV-2 NTD, RBD, and RBD-SD1 Regions

The domain structure of the SARS-CoV-2 spike was clearly evident in our cryo-EM structure and consistent with published accounts (Walls et al., 2020; Wrapp et al., 2020b). Based on these structures, we created constructs incorporating NTD, RBD, and RBD-SD1 regions as separate molecular probes (Figure 4). Transient transfection yield for each of these constructs was >5 mg/L. Both NTD and RBD eluted as a single peak on size-exclusion chromatography and exhibited a single band on SDS-PAGE (Figures 5A and 5B). RBD-SD1 eluted as two peaks

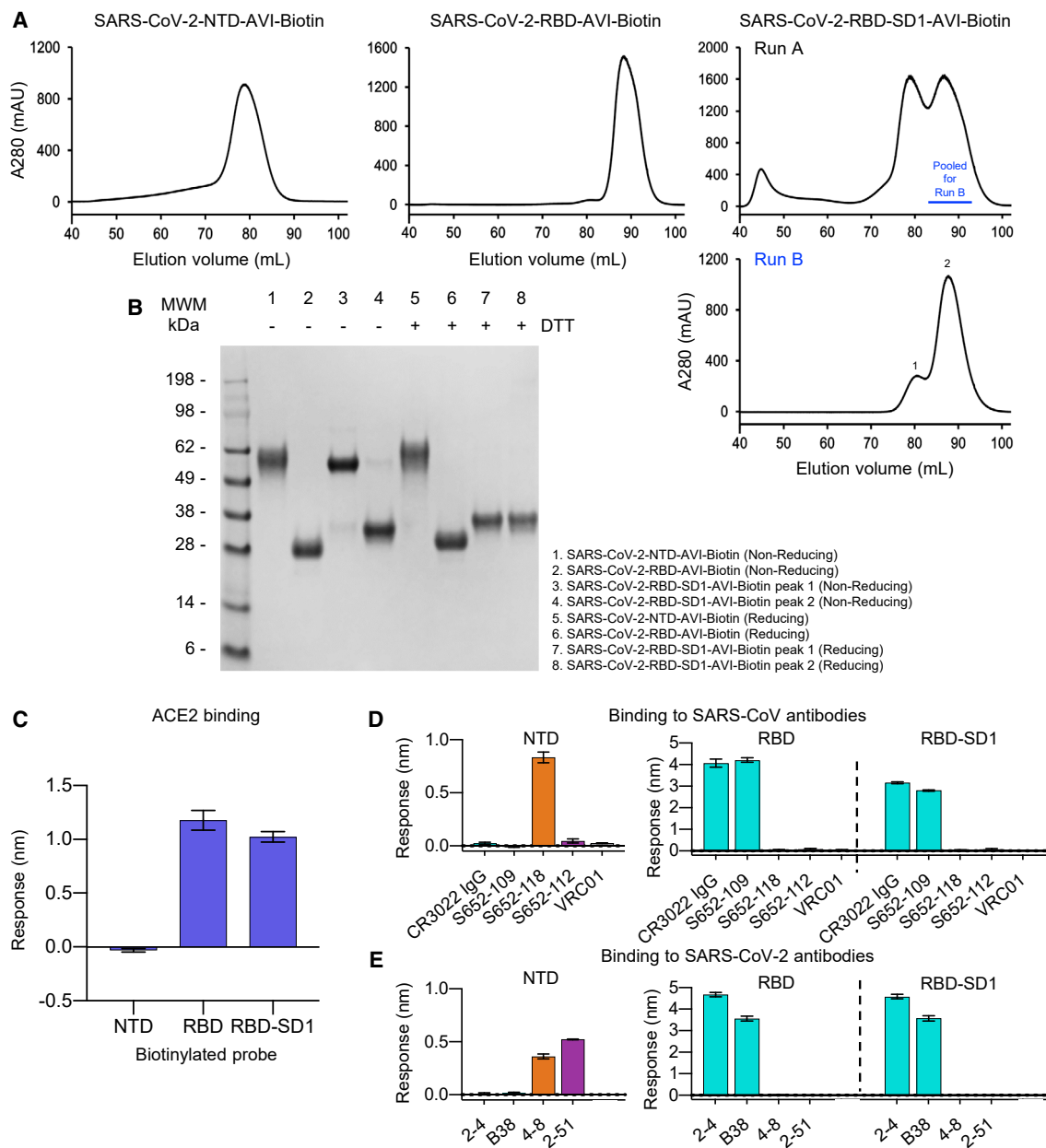


Figure 5. Physical Properties and Antigenic Characteristics of Molecular Probes Comprising SARS-CoV-2 NTD, RBD, and RBD-SD1 Domains

(A) Size-exclusion chromatography of biotinylated NTD, RBD, and RBD-SD1 molecular probes.

(B) SDS-PAGE of NTD, RBD, and RBD-SD1 molecular probes. RBD-SD1 peak 1 appeared to be partially disulfide linked and was therefore removed from further analysis; RBD-SD1 thus refers to the monomeric peak 2.

(C) Binding of receptor ACE2 to both RBD and RBD-SD1 probes.

(D) Binding of SARS-CoV antibodies to NTD (left) and RBD (right) probes. Both RBD and RBD-SD1 probes bound to antibodies CR3022 and S652-109, while the NTD probe specifically interacted with antibody S652-118. HIV-1 antibody VRC01 was used as control.

(E) Binding of SARS-CoV-2 antibodies to NTD (left) and RBD (right) probes. Antibodies 4-8 and 2-51 showed specific binding to the NTD probe. Antibodies 2-4 and B38 showed specific binding to RBD and RBD-SD1 probes.

Error bars represent standard deviation of triplicate measurements. See also [Figure S2](#).

on size-exclusion chromatography: a disulfide-bonded dimer and a monomer (Figures 5A and 5B). We chose the monomeric form for further studies, as there is no biological basis for a higher

association. Receptor recognition of these domain probes was specific for each construct, with ACE2 binding to RBD and RBD-SD1 probes, but not to the NTD probe (Figure 5C).

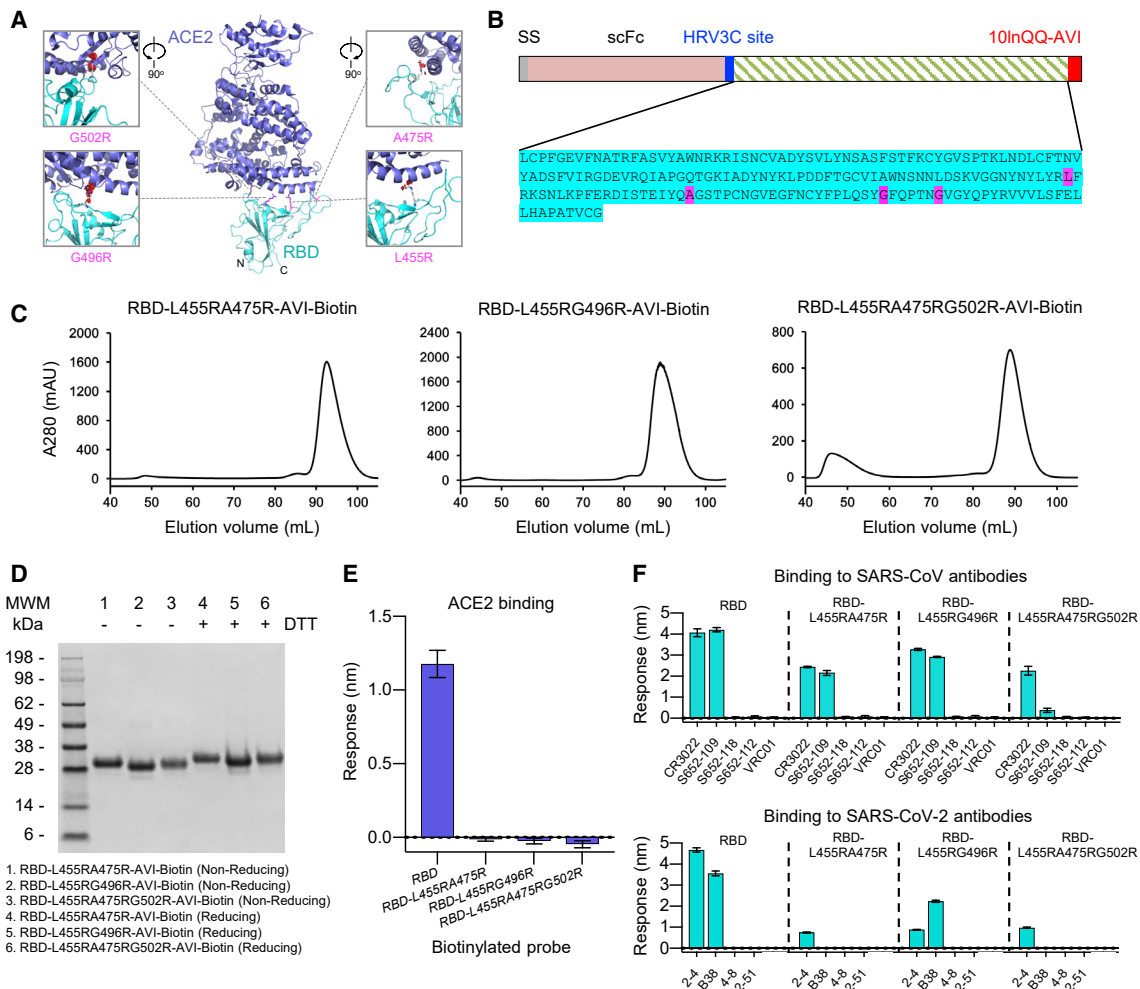


Figure 6. Molecular Probes Comprising Specific Mutations for Knocking Out ACE2 Interaction with RBD

(A) Structural model of the RBD-ACE2 complex, with inset panels highlighting RBD mutations designed to reduce ACE2 recognition. ACE2 and RBD are shown in cartoon representation and colored blue and cyan, respectively. Arg mutations are shown in stick representation, with potential clashes with ACE2 highlighted with red discs.

(B) Schematic and sequence of mutant RBD probes with sites mutated to Arg highlighted in magenta.

(C) Size-exclusion chromatography of RBDs with mutations altering ACE2 binding.

(D) SDS-PAGE of mutant RBD probes with and without reducing agent as indicated.

(E) Binding to receptor ACE2. All the knockout mutations abolished RBD binding to the ACE2 receptor.

(F) Binding to antibodies. Both SARS-CoV (top) and SARS-CoV-2 (bottom) antibodies were tested. Binding to all the SARS-CoV-2 antibodies and to SARS-CoV antibody S652-109 was reduced or abolished by the knockout mutations. Binding to CR3022, whose epitope is not on the ACE2-binding site, was not significantly affected. All binding was assessed using 7.5 $\mu\text{g}/\text{mL}$ RBD-L455RA475R, 80 $\mu\text{g}/\text{mL}$ RBD-L455RG496R, or 15 $\mu\text{g}/\text{mL}$ RBD-L455RA475RG502R to account for varying biotinylation levels among the mutants. Receptor or antibodies were at 500 nM. HIV-1 antibody VRC01 was used as a negative control. Error bars represent standard deviation of triplicate measurements.

See also [Figure S2](#) and [Table S1](#).

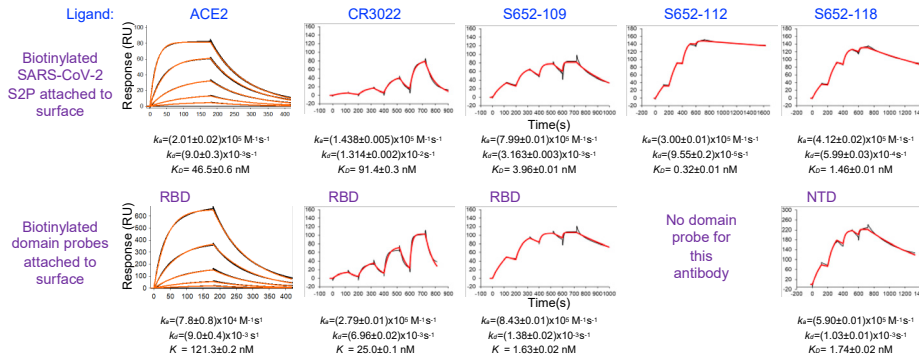
Similarly, SARS-CoV antibodies CR3022 and S652-109 recognized RBD and RBD-SD1, while S652-112 showed no binding to these two probes ([Figure 5D](#)) and antibody S652-118 recognized only the NTD probe ([Figure 5D](#)). Binding assays with SARS-CoV-2 antibodies further confirmed antigenic specificities of these domain probes ([Figure 5E](#)). Notably, the 2-51 antibody did recognize the NTD probe, consistent with its clustering, but not in its reported NTD recognition ([Liu et al., 2020a](#)). Overall,

these results indicate that the truncated domain probes folded properly and retained the native conformation as on the full-length S2P probe.

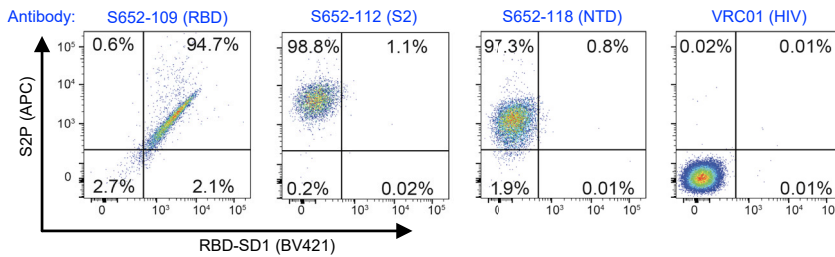
Molecular Probes Comprising Specific Knockouts of ACE2 Interaction with RBD

Structural information can define not only domain boundaries but also biological interfaces. Based on the structure of the

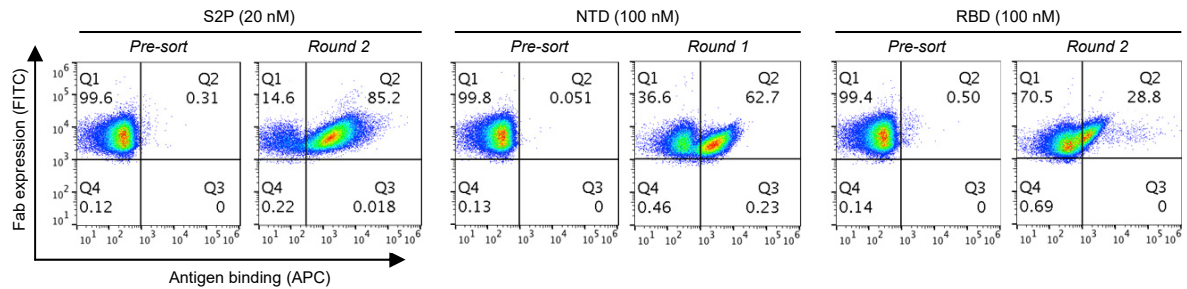
A SPR definition of ligand and antibody binding kinetics and affinity



B Probe sorting of yeast expressing specific antibodies



C Probe sorting of VH:VL yeast display library comprising antibodies from a convalescent COVID-19 donor



D Probe sorting of B cells from convalescent PBMCs

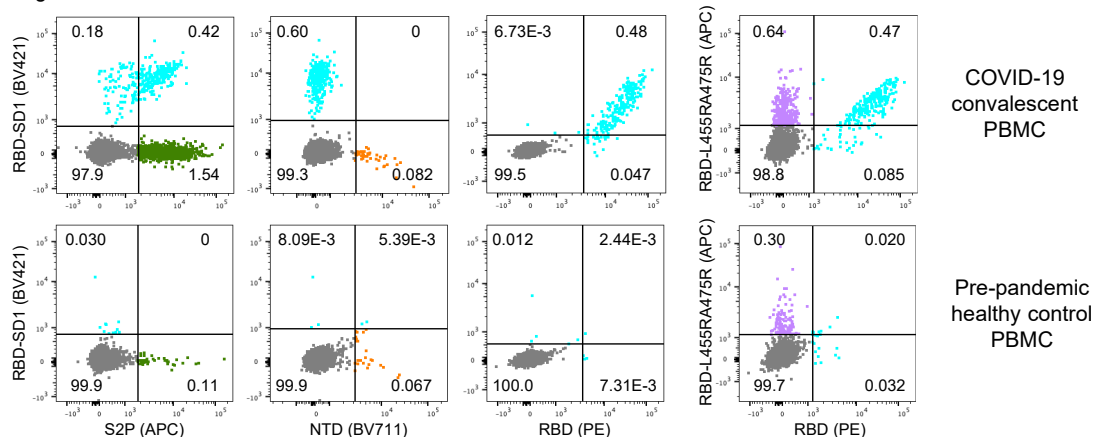


Figure 7. Validation of Biotinylated Probes

(A) SPR standard kinetic experiments for ACE2 and single-cycle kinetic experiments for Fabs CR3022, S652-109, S652-112, and S652-118 binding over biotinylated spike (top row) and biotinylated RBD or biotinylated NTD (bottom row) loaded onto a streptavidin sensor chip. Black traces represent the experimental data, and the red traces represent the fit to a 1:1 interaction model. The error in each measurement represents the error of the fit.

(B) Binding of yeast expressing SARS-CoV cross-reactive Fabs to SARS-CoV-2 antigenic probes. HIV envelope-targeting VRC01 Fab was used as a negative control.

(legend continued on next page)

RBD domain with ACE2 (Lan et al., 2020) (Figure 6A), we designed constructs with ACE2-interface residues mutated to Arg to knockout ACE2 affinity (Figure 6B). We expressed and purified two double-Arg mutants (RBD-L455RA475R-AVI and RBD-L455RG496R-AVI) and one triple-Arg mutant (RBD-L455RA475RG502R-AVI). All three eluted in a single peak on size-exclusion chromatography and exhibited a single band on SDS-PAGE (Figures 6C and 6D). All three mutants completely ablated ACE2 binding as designed (Figure 6E). By contrast, CR3022 recognition by all three mutants was mostly retained as the epitope of CR3022 and ACE2-binding site are located at different locations on RBD; S652-109 recognition by the double-Arg mutants was mostly retained and its recognition by RBD-L455RA475RG502R-AVI was reduced but at a detectable level, indicating a potential epitope overlapping the G502 region (Figure 6F). SARS-CoV-2 antibody B38 binding to the RBD probes was abolished by the L455RA475R mutations, while that to the RBD-L455RG496R-AVI probe was partially retained, indicating the critical role of the A475R mutation. By contrast, binding to 2-4 was reduced, but not abolished (Figure 6F), by all mutations, consistent with the structural data that the epitope of 2-4 only partially overlaps with the ACE2-binding site (Liu et al., 2020a). Our results indicated that the ACE2-interface mutant probes can be used to specifically distinguish antibodies targeting the ACE2-binding site and other epitopes on the RBD.

Validation of Biotinylated Probes

To assess the molecular probes for their quality and function, we first performed kinetic analyses of ACE2 receptor and antibodies binding to the probes by SPR (Figure 7A). Purified biotinylated probes were immobilized on streptavidin sensor chip surface, and ACE2 and antibodies were in the mobile phase. ACE2 bound the full-length ectodomain probe S2P, with a K_D of 46.5 nM, and its affinity to the isolated RBD domain probe was somewhat lower, with a K_D of 121 nM. We found the S2P probe to be sensitive to chip regeneration required to remove antibody, so we used single-cycle kinetics to analyze the interaction with the Fabs of antibodies CR3022, S652-109, S652-112, and S652-118. These all bound SARS-CoV-2 S2P probe with high affinity (Figure 7A, top row). Interestingly, the binding on-rates for all three of the antibodies were comparable, but the off-rates varied. CR3022, an antibody known to bind RBD, but not neutralize the SARS-CoV-2 virus (Yuan et al., 2020), bound to SARS-CoV-2 S2P at a lower affinity than ACE2 (91.4 versus 46.5 nM, respectively), although CR3022 had a higher affinity to the RBD probe (25.0 nM) than to S2P (91.4 nM). Another RBD-binding non-neutralizing antibody, S652-109, bound to the RBD and S2P probes at 1.63 and 3.96 nM, respectively. Antibody S652-112, also non-neutralizing, did not bind NTD or RBD probes (Figure 5D), but it did bind the S2P probe with a K_D of 0.32 nM, consistent with it being S2 directed. An NTD-specific antibody, S652-118, which does have some neutralizing capacity, bound

NTD and S2P probes at 1.74 and 1.46 nM, respectively. These results confirm that the biotinylated probes have the binding specificity for the receptor and antibodies and are functioning properly as expected.

We next tested the probes for sorting antigen-specific yeast cells displaying SARS-CoV-2 antibodies (Figures 7B, S4, and S5). We expressed antibodies S652-109, S652-112, and S652-118 on yeast cell surface. The biotinylated probes, S2P, RBD-SD1, and the ACE2-knockout triple-Arg mutant RBD-L455RA475RG502R, were freshly labeled with fluorochromes and used to sort the yeast cells. As expected, the S2P probe recognized all cells expressing S652-109, S652-112, and S652-118, but not those with the control antibody, whereas the RBD-SD1 probes recognized only cells expressing S652-109 (Figures 7B and S5). The triple-Arg mutant RBD-L455RA475RG502R also recognized S652-109 (Figure S5), consistent with the BLI binding assay described above that showed residual binding was retained (Figure 6F). These results confirm the utility of the probes for sorting cells expressing SARS-CoV-2 spike-specific antibodies on cell surface.

Having established the cell-sorting utility of the probes, we next set out to test the probes in sorting and enriching natively paired V_H : V_L yeast display libraries of convalescent COVID-19 donors for SARS-CoV-2 spike-specific antibodies (Figures 7C and S6) (Wang et al., 2018a). Depending on the initial level of antigen-specific antibodies present, just one or two rounds of sorting and enrichment could increase the antigen-specific cells by several orders of magnitude, indicating substantial utility of the probes for cell sorting.

To further demonstrate the utility of the probes in sorting of human B cells, we obtained peripheral blood mononuclear cells (PBMCs) from a convalescent SARS-CoV-2 affected individual and sorted the cells with fluorochrome-labeled probes (Figures 7D and S7). S2P-positive, RBD-SD1-positive, and RBD-positive B cells were identified from the PBMCs of the affected individual, but not from pre-pandemic healthy control PBMCs (Figure 7D, left three panels). The double-Arg mutant RBD-L455RA475R, in contrast, recognized only ~2-fold more B cells than the control (Figure 7D, far right panel), with only a small proportion of B cells not binding mutant versus RBD-SD1 (Figure 7D, compare third and fourth panels).

Overall, the designed probes were found to be functional in SPR and in sorting yeast cells or B cells with spike-reactive antibodies.

DISCUSSION

Molecular probes comprising key targets such as the SARS-CoV-2 spike and its domains can be of broad utility. For vaccine development, such probes can be used to define and monitor the elicited responses, and for antibody characterization, such probes can serve as critical molecular tags, facilitating the

(C) Sorting of yeast cells encoding antibody transcripts from a convalescent COVID-19 donor with S2P-, NTD-, and RBD-based probes.

(D) Sorting of B cells from COVID-19 convalescent PBMCs. (Top row) PBMCs obtained from a SARS-CoV-2-infected subject 75 days after symptom onset were stained with surface antibodies and probes as outlined in the STAR Methods to allow for identification and specificity-determination of SARS-CoV-2 spike-specific IgG+ and IgA+ B cells. (Bottom row) PBMCs obtained pre-pandemic from a healthy donor serve as a control for background binding of the probes. See also Figures S4–S7.

identification of the highly effective antibodies that could be used for passive therapy (Cao et al., 2020; reviewed in Casadevall et al., 2004; Graham and Ambrosino, 2015; Walker and Burton, 2018). In diagnostics, they can be used to assess sera reactivity and to provide sensitive markers of infection (Perera et al., 2020; Yan et al., 2020b; Zhao et al., 2020). In pathogenesis, they can assist in delineating susceptible cells that virus might infect or in tracking viral variants, including those that might have selective advantages (Korber et al., 2020). Here, we show how structure-based design coupled to incorporation of (1) a purification tag-based construct, (2) a sequence-specific protease, and (3) a sequence-specific biotin ligase enables streamlined probe development.

For probe construction, we used a process incorporating the “cut-and-paste” assembly of necessary components, using an N-terminal purification tag and sequence stretches targeted by sequence-specific enzymes: the HRV3C protease and biotin ligase. Other sequence-specific cleavage sites such as thrombin could be incorporated, to further control the presence of components surrounding the target protein of interest. Such protease-specific cleavage, however, can lead to the addition of residual amino acids at resultant N and C termini after protease cleavage; we note in this context that an N-terminal HRV3C site appends only a dipeptide, Gly-Pro, to the N terminus of the liberated target. Importantly, structure of the target protein can define domain boundaries, allowing for separate probes of specific domains or domain combinations.

The structure-based methods we describe here for probe construction may allow for the assessment of immune responses of other type 1 fusion machines. We previously created hemagglutinin trimer probes with a Y96F mutation (Whittle et al., 2014) and used them to identify broadly neutralizing antibodies against influenza (Joyce et al., 2016). We also created Ebolavirus trimer probes that could be used to identify protective neutralizing antibodies against Sudan outbreak Ebolavirus strain (Corti et al., 2016; Gaudinski et al., 2019; Misasi et al., 2016). And we previously used a biotinylated envelope “SOSIP” probe to identify broadly neutralizing, fusion peptide-directed antibodies against HIV-1 (Kong et al., 2016). Overall, the cut-and-paste structure-based design described here should be easily adapted to the streamlined development of molecular probes against not only these pathogens, but also emerging pathogens, as shown here for SARS-CoV-2.

STAR★METHODS

Detailed methods are provided in the online version of this paper and include the following:

- **KEY RESOURCES TABLE**
- **RESOURCE AVAILABILITY**
 - Lead Contact
 - Materials Availability
 - Data and Code Availability
- **EXPERIMENTAL MODEL AND SUBJECT DETAILS**
 - Patient samples
 - Cell lines
- **METHOD DETAILS**

- Construction of expression plasmids for SARS-CoV-2 probes
- Expression and preparation of SARS-CoV-2 probes
- Expression and preparation of the ACE2 receptor
- Expression and preparation of antibodies
- Bio-Layer Interferometry
- Surface plasmon resonance
- Negative-stain electron microscopy
- Cryo-EM data collection and processing
- Cryo-EM model fitting
- Probe conjugation
- Monoclonal yeast display analysis
- Experimental sorting of natively paired antibody heavy:light yeast display libraries
- PBMC B cell stain

● QUANTIFICATION AND STATISTICAL ANALYSIS

SUPPLEMENTAL INFORMATION

Supplemental Information can be found online at <https://doi.org/10.1016/j.celrep.2020.108322>.

ACKNOWLEDGMENTS

We thank R. Grassucci, Y.-C. Chi, and Z. Zhang from the Cryo-EM Center at Columbia University for assistance with cryo-EM data collection; M.G. Joyce for antibody CR3022; J. Stuckey for assistance with figures; and members of the Virology Laboratory and Vector Core, Vaccine Research Center, for discussions and comments on the manuscript. Support for this work was provided by the Intramural Research Program of the Vaccine Research Center, National Institute of Allergy and Infectious Diseases (NIAID). Support for this work was also provided by COVID-19 Fast Grants, the Jack Ma Foundation, the Self Graduate Fellowship Program, and NIH grants DP5OD023118, R21AI143407, and R21AI144408. Some of this work was performed at the Columbia University Cryo-EM Center at the Zuckerman Institute and some at the Simons Electron Microscopy Center (SEMC) and National Center for Cryo-EM Access and Training (NCCAT) located at the New York Structural Biology Center, supported by grants from the Simons Foundation (SF349247), NYSTAR, and the NIH National Institute of General Medical Sciences (GM103310).

AUTHOR CONTRIBUTIONS

T.Z. designed the probes; T.Z., I-T.T., and A.S.O. produced the probes; G.C. and J.G. determined cryo-EM structure of S2P; T.Z. and A.N. performed Octet antigenic assessment; W.S. provided ACE2; Y.T. performed negative-stain EM; L.W., K.S.C., and Y.Z. provided antibodies S652-109, S652-112, and S652-118; S.W. assisted with data analysis and manuscript assembly; B.Z. produced antibody CR3022; P.S.K. carried out SPR; Y.P., J.M., and N.J.S. performed monoclonal yeast display analysis; B.B.B., A.S.F., L.L., S.N.L.A., B.M., M.O.d.S., X.P., P.W., J.R.W., M.Y., D.D.H., and B.J.D. carried out natively paired antibody yeast display analysis; E.P., A.D., L.C., O.M.A., K.S.C., T.R., and B.S.G. preformed PBMC B cell staining analysis; J.R.M. supervised ACE2 and antibodies S652-109, S652-112, and S652-118 production; L.S. supervised SPR and cryo-EM structural analyses; T.Z., L.S., and P.D.K. oversaw the project—and with I-T.T., A.S.O., G.C., J.G., Y.T., S.W., J.M., B.J.D., and T.R.—provided a first draft of the manuscript, with all authors providing revisions and comments.

DECLARATION OF INTERESTS

The authors declare no competing interest.

Received: June 21, 2020
Revised: September 16, 2020
Accepted: October 7, 2020
Published: October 12, 2020

REFERENCES

Adams, P.D., Gopal, K., Grosse-Kunstleve, R.W., Hung, L.W., Ioerger, T.R., McCoy, A.J., Moriarty, N.W., Pai, R.K., Read, R.J., Romo, T.D., et al. (2004). Recent developments in the PHENIX software for automated crystallographic structure determination. *J. Synchrotron Radiat.* *11*, 53–55.

Antoniou, G., Papakyriacou, I., and Papanephytous, C. (2017). Optimization of Soluble Expression and Purification of Recombinant Human Rhinovirus Type-14 3C Protease Using Statistically Designed Experiments: Isolation and Characterization of the Enzyme. *Mol. Biotechnol.* *59*, 407–424.

Barad, B.A., Echols, N., Wang, R.Y., Cheng, Y., DiMaio, F., Adams, P.D., and Fraser, J.S. (2015). EMRinger: side chain-directed model and map validation for 3D cryo-electron microscopy. *Nat. Methods* *12*, 943–946.

Brouwer, P.J.M., Caniels, T.G., van der Straten, K., Snitselaar, J.L., Aldon, Y., Bangaru, S., Torres, J.L., Okba, N.M.A., Claireaux, M., Kerster, G., et al. (2020). Potent neutralizing antibodies from COVID-19 patients define multiple targets of vulnerability. *Science* *369*, 643–650.

Callaway, E. (2020). The race for coronavirus vaccines: a graphical guide. *Nature* *580*, 576–577.

Callaway, E., Cyranoski, D., Mallapaty, S., Stoye, E., and Tollefson, J. (2020). The coronavirus pandemic in five powerful charts. *Nature* *579*, 482–483.

Cao, Y., Su, B., Guo, X., Sun, W., Deng, Y., Bao, L., Zhu, Q., Zhang, X., Zheng, Y., Geng, C., et al. (2020). Potent neutralizing antibodies against SARS-CoV-2 identified by high-throughput single-cell sequencing of convalescent patients' B cells. *Cell* *182*, 73–84.

Casadevall, A., Dadachova, E., and Pirofski, L.A. (2004). Passive antibody therapy for infectious diseases. *Nat. Rev. Microbiol.* *2*, 695–703.

Chen, X., Li, R., Pan, Z., Qian, C., Yang, Y., You, R., Zhao, J., Liu, P., Gao, L., Li, Z., et al. (2020). Human monoclonal antibodies block the binding of SARS-CoV-2 spike protein to angiotensin converting enzyme 2 receptor. *Cell. Mol. Immunol.* *17*, 647–649.

Chi, X., Yan, R., Zhang, J., Zhang, G., Zhang, Y., Hao, M., Zhang, Z., Fan, P., Dong, Y., Yang, Y., et al. (2020). A potent neutralizing human antibody reveals the N-terminal domain of the Spike protein of SARS-CoV-2 as a site of vulnerability. *bioRxiv*, 2020.05.08.083964.

Cordingley, M.G., Callahan, P.L., Sardana, V.V., Garsky, V.M., and Colonno, R.J. (1990). Substrate requirements of human rhinovirus 3C protease for peptide cleavage in vitro. *J. Biol. Chem.* *265*, 9062–9065.

Corti, D., Misasi, J., Mulangu, S., Stanley, D.A., Kanekiyo, M., Wollen, S., Ploquin, A., Doria-Rose, N.A., Staube, R.P., Bailey, M., et al. (2016). Protective monotherapy against lethal Ebola virus infection by a potentially neutralizing antibody. *Science* *351*, 1339–1342.

Cucinotta, D., and Vanelli, M. (2020). WHO Declares COVID-19 a Pandemic. *Acta Biomed.* *91*, 157–160.

Davis, I.W., Murray, L.W., Richardson, J.S., and Richardson, D.C. (2004). MOLPROBITY: structure validation and all-atom contact analysis for nucleic acids and their complexes. *Nucleic Acids Res.* *32*, W615–W619.

DeKosky, B.J., Ippolito, G.C., Deschner, R.P., Lavinder, J.J., Wine, Y., Rawlings, B.M., Varadarajan, N., Giesecke, C., Dörner, T., Andrews, S.F., et al. (2013). High-throughput sequencing of the paired human immunoglobulin heavy and light chain repertoire. *Nat. Biotechnol.* *31*, 166–169.

DeKosky, B.J., Kojima, T., Rodin, A., Charab, W., Ippolito, G.C., Ellington, A.D., and Georgiou, G. (2015). In-depth determination and analysis of the human paired heavy- and light-chain antibody repertoire. *Nat. Med.* *21*, 86–91.

Efimov, V.P., Nepluev, I.V., Sobolev, B.N., Zurabishvili, T.G., Schulthess, T., Lustig, A., Engel, J., Haener, M., Aebi, U., Venyaminov SYu, et al. (1994). Fibrin encoded by bacteriophage T4 gene wac has a parallel triple-stranded α -helical coiled-coil structure. *J. Mol. Biol.* *242*, 470–486.

Emley, P., and Cowtan, K. (2004). Coot: model-building tools for molecular graphics. *Acta Crystallogr. D Biol. Crystallogr.* *60*, 2126–2132.

Gaudinski, M.R., Coates, E.E., Novik, L., Widge, A., Houser, K.V., Burch, E., Holman, L.A., Gordon, I.J., Chen, G.L., Carter, C., et al.; VRC 608 Study Team (2019). Safety, tolerability, pharmacokinetics, and immunogenicity of the therapeutic monoclonal antibody mAb114 targeting Ebola virus glycoprotein (VRC 608): an open-label phase 1 study. *Lancet* *393*, 889–898.

Graham, B.S., and Ambrosino, D.M. (2015). History of passive antibody administration for prevention and treatment of infectious diseases. *Curr. Opin. HIV AIDS* *10*, 129–134.

Graham, R.L., Donaldson, E.F., and Baric, R.S. (2013). A decade after SARS: strategies for controlling emerging coronaviruses. *Nat. Rev. Microbiol.* *11*, 836–848.

Hoffmann, M., Kleine-Weber, H., Schroeder, S., Kruger, N., Herrler, T., Erichsen, S., Schiergens, T.S., Herrler, G., Wu, N.H., Nitsche, A., et al. (2020). SARS-CoV-2 Cell Entry Depends on ACE2 and TMPRSS2 and Is Blocked by a Clinically Proven Protease Inhibitor. *Cell* *181*, 271–280.

Jäger, V., Büsow, K., Wagner, A., Weber, S., Hust, M., Frenzel, A., and Schirrmann, T. (2013). High level transient production of recombinant antibodies and antibody fusion proteins in HEK293 cells. *BMC Biotechnol.* *13*, 52.

Jiang, S., Hillyer, C., and Du, L. (2020). Neutralizing Antibodies against SARS-CoV-2 and Other Human Coronaviruses. *Trends Immunol.* *41*, 355–359.

Johnson, G., and Wu, T.T. (2000). Kabat database and its applications: 30 years after the first variability plot. *Nucleic Acids Res.* *28*, 214–218.

Joyce, M.G., Wheatley, A.K., Thomas, P.V., Chuang, G.Y., Soto, C., Bailer, R.T., Druz, A., Georgiev, I.S., Gillespie, R.A., Kanekiyo, M., et al.; NISC Comparative Sequencing Program (2016). Vaccine-Induced Antibodies that Neutralize Group 1 and Group 2 Influenza A Viruses. *Cell* *166*, 609–623.

Ju, B., Zhang, Q., Ge, J., Wang, R., Sun, J., Ge, X., Yu, J., Shan, S., Zhou, B., Song, S., et al. (2020). Human neutralizing antibodies elicited by SARS-CoV-2 infection. *Nature* *584*, 115–119.

Kong, R., Xu, K., Zhou, T., Acharya, P., Lemmin, T., Liu, K., Ozorowski, G., Soto, C., Taft, J.D., Bailer, R.T., et al. (2016). Fusion peptide of HIV-1 as a site of vulnerability to neutralizing antibody. *Science* *352*, 828–833.

Korber, B., Fischer, W.M., Gnanakaran, S., Yoon, H., Theiler, J., Abfalterer, W., Hengartner, N., Giorgi, E.E., Bhattacharya, T., Foley, B., et al.; Sheffield COVID-19 Genomics Group (2020). Tracking Changes in SARS-CoV-2 Spike: Evidence that D614G Increases Infectivity of the COVID-19 Virus. *Cell* *182*, 812–827.e19.

Lagerman, C.E., López Acevedo, S.N., Fahad, A.S., Hailemariam, A.T., Madan, B., and DeKosky, B.J. (2019). Ultrasonically-guided flow focusing generates precise emulsion droplets for high-throughput single cell analyses. *J. Biosci. Bioeng.* *128*, 226–233.

Lan, J., Ge, J., Yu, J., Shan, S., Zhou, H., Fan, S., Zhang, Q., Shi, X., Wang, Q., Zhang, L., and Wang, X. (2020). Structure of the SARS-CoV-2 spike receptor-binding domain bound to the ACE2 receptor. *Nature* *581*, 215–220.

Liu, L., Xie, J., Sun, J., Han, Y., Zhang, C., Fan, H., Liu, Z., Qiu, Z., He, Y., and Li, T. (2011). Longitudinal profiles of immunoglobulin G antibodies against severe acute respiratory syndrome coronavirus components and neutralizing activities in recovered patients. *Scand. J. Infect. Dis.* *43*, 515–521.

Liu, L., Wang, P., Nair, M.S., Yu, J., Rapp, M., Wang, Q., Luo, Y., Chan, J.F., Sahi, V., Figueroa, A., et al. (2020a). Potent neutralizing antibodies against multiple epitopes on SARS-CoV-2 spike. *Nature* *584*, 450–456.

Liu, X., Gao, F., Gou, L., Chen, Y., Gu, Y., Ao, L., Shen, H., Hu, Z., Guo, X., and Gao, W. (2020b). Neutralizing Antibodies Isolated by a site-directed Screening have Potent Protection on SARS-CoV-2 Infection. *bioRxiv*, 2020.05.03.074914.

Mastrorade, D.N. (2005). Automated electron microscope tomography using robust prediction of specimen movements. *J. Struct. Biol.* *152*, 36–51.

McDaniel, J.R., DeKosky, B.J., Tanno, H., Ellington, A.D., and Georgiou, G. (2016). Ultra-high-throughput sequencing of the immune receptor repertoire from millions of lymphocytes. *Nat. Protoc.* *11*, 429–442.

- Miroshnikov, K.A., Marusich, E.I., Cerritelli, M.E., Cheng, N., Hyde, C.C., Steven, A.C., and Mesyanzhinov, V.V. (1998). Engineering trimeric fibrous proteins based on bacteriophage T4 adhesins. *Protein Eng.* *11*, 329–332.
- Misasi, J., Gilman, M.S., Kanekiyo, M., Gui, M., Cagigi, A., Mulangu, S., Corti, D., Ledgerwood, J.E., Lanzavecchia, A., Cunningham, J., et al. (2016). Structural and molecular basis for Ebola virus neutralization by protective human antibodies. *Science* *351*, 1343–1346.
- Ou, X., Liu, Y., Lei, X., Li, P., Mi, D., Ren, L., Guo, L., Guo, R., Chen, T., Hu, J., et al. (2020). Characterization of spike glycoprotein of SARS-CoV-2 on virus entry and its immune cross-reactivity with SARS-CoV. *Nat. Commun.* *11*, 1620.
- Pallesen, J., Wang, N., Corbett, K.S., Wrapp, D., Kirchdoerfer, R.N., Turner, H.L., Cottrell, C.A., Becker, M.M., Wang, L., Shi, W., et al. (2017). Immunogenicity and structures of a rationally designed prefusion MERS-CoV spike antigen. *Proc. Natl. Acad. Sci. USA* *114*, E7348–E7357.
- Perera, R.A., Mok, C.K., Tsang, O.T., Lv, H., Ko, R.L., Wu, N.C., Yuan, M., Leung, W.S., Chan, J.M., Chik, T.S., et al. (2020). Serological assays for severe acute respiratory syndrome coronavirus 2 (SARS-CoV-2), March 2020. *Euro Surveill.* *25*, 2000421.
- Pettersen, E.F., Goddard, T.D., Huang, C.C., Couch, G.S., Greenblatt, D.M., Meng, E.C., and Ferrin, T.E. (2004). UCSF Chimera—a visualization system for exploratory research and analysis. *J. Comput. Chem.* *25*, 1605–1612.
- Pinto, D., Park, Y.-J., Beltramello, M., Walls, A.C., Tortorici, M.A., Bianchi, S., Jaconi, S., Culp, K., Zatta, F., De Marco, A., et al. (2020). Cross-neutralization of SARS-CoV-2 by a human monoclonal SARS-CoV antibody. *Nature* *583*, 290–295.
- Punjani, A., Rubinstein, J.L., Fleet, D.J., and Brubaker, M.A. (2017). cryo-SPARC: algorithms for rapid unsupervised cryo-EM structure determination. *Nat. Methods* *14*, 290–296.
- Ridgway, J.B., Presta, L.G., and Carter, P. (1996). ‘Knobs-into-holes’ engineering of antibody CH3 domains for heavy chain heterodimerization. *Protein Eng.* *9*, 617–621.
- Robbiani, D.F., Gaebler, C., Muecksch, F., Lorenzi, J.C.C., Wang, Z., Cho, A., Agudelo, M., Barnes, C.O., Gazumyan, A., Finkin, S., et al. (2020). Convergent antibody responses to SARS-CoV-2 in convalescent individuals. *Nature* *584*, 437–442.
- Rogers, T.F., Zhao, F., Huang, D., Beutler, N., Burns, A., He, W.T., Limbo, O., Smith, C., Song, G., Woehl, J., et al. (2020). Isolation of potent SARS-CoV-2 neutralizing antibodies and protection from disease in a small animal model. *Science* *369*, 956–963.
- Rohou, A., and Grigorieff, N. (2015). CTFFIND4: Fast and accurate defocus estimation from electron micrographs. *J. Struct. Biol.* *192*, 216–221.
- Scheres, S.H. (2012). RELION: implementation of a Bayesian approach to cryo-EM structure determination. *J. Struct. Biol.* *180*, 519–530.
- Seydoux, E., Homad, L.J., MacCamy, A.J., Parks, K.R., Hurlburt, N.K., Jennein, M.F., Akins, N.R., Stuart, A.B., Wan, Y.-H., Feng, J., et al. (2020). Characterization of neutralizing antibodies from a SARS-CoV-2 infected individual. *bioRxiv*, 2020.05.12.091298.
- Shen, Y., Maupetit, J., Derreumaux, P., and Tufféry, P. (2014). Improved PEP-FOLD Approach for Peptide and Mini-protein Structure Prediction. *J. Chem. Theory Comput.* *10*, 4745–4758.
- Suloway, C., Pulokas, J., Fellmann, D., Cheng, A., Guerra, F., Quispe, J., Stagg, S., Potter, C.S., and Carragher, B. (2005). Automated molecular microscopy: the new Legation system. *J. Struct. Biol.* *151*, 41–60.
- Thévenet, P., Shen, Y., Maupetit, J., Guyon, F., Derreumaux, P., and Tufféry, P. (2012). PEP-FOLD: an updated de novo structure prediction server for both linear and disulfide bonded cyclic peptides. *Nucleic Acids Res.* *40*, W288–W293.
- Tian, X., Li, C., Huang, A., Xia, S., Lu, S., Shi, Z., Lu, L., Jiang, S., Yang, Z., Wu, Y., and Ying, T. (2020). Potent binding of 2019 novel coronavirus spike protein by a SARS coronavirus-specific human monoclonal antibody. *Emerg. Microbes Infect.* *9*, 382–385.
- Voss, N.R., Yoshioka, C.K., Radermacher, M., Potter, C.S., and Carragher, B. (2009). DoG Picker and TiltPicker: software tools to facilitate particle selection in single particle electron microscopy. *J. Struct. Biol.* *166*, 205–213.
- Walker, L.M., and Burton, D.R. (2018). Passive immunotherapy of viral infections: ‘super-antibodies’ enter the fray. *Nat. Rev. Immunol.* *18*, 297–308.
- Walls, A.C., Park, Y.J., Tortorici, M.A., Wall, A., McGuire, A.T., and Velesler, D. (2020). Structure, Function, and Antigenicity of the SARS-CoV-2 Spike Glycoprotein. *Cell* *181*, 281–292.
- Wang, B., DeKosky, B.J., Timm, M.R., Lee, J., Normandin, E., Misasi, J., Kong, R., McDaniel, J.R., Delidakis, G., Leigh, K.E., et al. (2018a). Functional interrogation and mining of natively paired human V_H:V_L antibody repertoires. *Nat. Biotechnol.* *36*, 152–155.
- Wang, C., Li, W., Drabek, D., Okba, N.M.A., van Haperen, R., Osterhaus, A.D.M.E., van Kuppeveld, F.J.M., Haagmans, B.L., Grosveld, F., and Bosch, B.J. (2020a). A human monoclonal antibody blocking SARS-CoV-2 infection. *Nat. Commun.* *11*, 2251.
- Wang, L., Shi, W., Chappell, J.D., Joyce, M.G., Zhang, Y., Kanekiyo, M., Becker, M.M., van Doremalen, N., Fischer, R., Wang, N., et al. (2018b). Importance of Neutralizing Monoclonal Antibodies Targeting Multiple Antigenic Sites on the Middle East Respiratory Syndrome Coronavirus Spike Glycoprotein To Avoid Neutralization Escape. *J. Virol.* *92*, e02002–17.
- Wang, Q., Zhang, Y., Wu, L., Niu, S., Song, C., Zhang, Z., Lu, G., Qiao, C., Hu, Y., Yuen, K.Y., et al. (2020b). Structural and Functional Basis of SARS-CoV-2 Entry by Using Human ACE2. *Cell* *181*, 894–904.
- Whittle, J.R., Wheatley, A.K., Wu, L., Lingwood, D., Kanekiyo, M., Ma, S.S., Narpala, S.R., Yassine, H.M., Frank, G.M., Yewdell, J.W., et al. (2014). Flow cytometry reveals that H5N1 vaccination elicits cross-reactive stem-directed antibodies from multiple Ig heavy-chain lineages. *J. Virol.* *88*, 4047–4057.
- Wrapp, D., De Vlieger, D., Corbett, K.S., Torres, G.M., Wang, N., Van Breedam, W., Roose, K., van Schie, L., VIB-CMB COVID-19 Response Team; and Hoffmann, M., et al. (2020a). Structural Basis for Potent Neutralization of Betacoronaviruses by Single-Domain Camelid Antibodies. *Cell* *181*, 1004–1015.
- Wrapp, D., Wang, N., Corbett, K.S., Goldsmith, J.A., Hsieh, C.L., Abiona, O., Graham, B.S., and McLellan, J.S. (2020b). Cryo-EM structure of the 2019-nCoV spike in the prefusion conformation. *Science* *367*, 1260–1263.
- Wu, X., Yang, Z.Y., Li, Y., Hogerkerp, C.M., Schief, W.R., Seaman, M.S., Zhou, T., Schmidt, S.D., Wu, L., Xu, L., et al. (2010). Rational design of envelope identifies broadly neutralizing human monoclonal antibodies to HIV-1. *Science* *329*, 856–861.
- Wu, X., Zhou, T., Zhu, J., Zhang, B., Georgiev, I., Wang, C., Chen, X., Longo, N.S., Louder, M., McKee, K., et al.; NISC Comparative Sequencing Program (2011). Focused evolution of HIV-1 neutralizing antibodies revealed by structures and deep sequencing. *Science* *333*, 1593–1602.
- Wu, Y., Wang, F., Shen, C., Peng, W., Li, D., Zhao, C., Li, Z., Li, S., Bi, Y., Yang, Y., et al. (2020). A noncompeting pair of human neutralizing antibodies block COVID-19 virus binding to its receptor ACE2. *Science* *368*, 1274–1278.
- Yan, R., Zhang, Y., Li, Y., Xia, L., Guo, Y., and Zhou, Q. (2020a). Structural basis for the recognition of SARS-CoV-2 by full-length human ACE2. *Science* *367*, 1444–1448.
- Yan, Y., Chang, L., and Wang, L. (2020b). Laboratory testing of SARS-CoV, MERS-CoV, and SARS-CoV-2 (2019-nCoV): Current status, challenges, and countermeasures. *Rev. Med. Virol.* *30*, e2106.
- Yongchen, Z., Shen, H., Wang, X., Shi, X., Li, Y., Yan, J., Chen, Y., and Gu, B. (2020). Different longitudinal patterns of nucleic acid and serology testing results based on disease severity of COVID-19 patients. *Emerg. Microbes Infect.* *9*, 833–836.
- Yuan, M., Wu, N.C., Zhu, X., Lee, C.D., So, R.T.Y., Lv, H., Mok, C.K.P., and Wilson, I.A. (2020). A highly conserved cryptic epitope in the receptor binding domains of SARS-CoV-2 and SARS-CoV. *Science* *368*, 630–633.
- Zeng, X., Li, L., Lin, J., Li, X., Liu, B., Kong, Y., Zeng, S., Du, J., Xiao, H., Zhang, T., et al. (2020). Isolation of a human monoclonal antibody specific for the receptor binding domain of SARS-CoV-2 using a competitive phage biopanning strategy. *Antib. Ther.* *3*, 95–100.

Zhang, K. (2016). Gctf: Real-time CTF determination and correction. *J. Struct. Biol.* *193*, 1–12.

Zhao, R., Li, M., Song, H., Chen, J., Ren, W., Feng, Y., Gao, G.F., Song, J., Peng, Y., Su, B., et al. (2020). Early detection of SARS-CoV-2 antibodies in COVID-19 patients as a serologic marker of infection. *Clin. Infect. Dis.*, ciaa523.

Zhou, G., and Zhao, Q. (2020). Perspectives on therapeutic neutralizing antibodies against the Novel Coronavirus SARS-CoV-2. *Int. J. Biol. Sci.* *16*, 1718–1723.

Zost, S.J., Gilchuk, P., Chen, R.E., Case, J.B., Reidy, J.X., Trivette, A., Nargi, R.S., Sutton, R.E., Suryadevara, N., Chen, E.C., et al. (2020). Rapid isolation and profiling of a diverse panel of human monoclonal antibodies targeting the SARS-CoV-2 spike protein. *Nat. Med.* *26*, 1422–1427.

STAR★METHODS

KEY RESOURCES TABLE

REAGENT or RESOURCE	SOURCE	IDENTIFIER
Antibodies		
2-4	Liu et al., 2020a	N/A
4-8	Liu et al., 2020a	N/A
2-51	Liu et al., 2020a	N/A
B38	Wu et al., 2020	N/A
CR3022	Yuan et al., 2020	N/A
S652-109	This study	N/A
S652-112	This study	N/A
S652-118	This Study	N/A
VRC01	Wu et al., 2010	N/A
Chemicals, Peptides, and Recombinant Proteins		
Superdex200 10/300GL Column	GE Healthcare Life Sciences	Cat# 28990944
MabSelect SuRe Protein A Resin	GE Healthcare Life Sciences	Cat# 17543802
SARS-CoV-2-S2P-AVI	This study	N/A
SARS-CoV-2-NTD-AVI	This study	N/A
SARS-CoV-2-RBD-AVI	This study	N/A
SARS-CoV-2-RBD-SD1-AVI	This study	N/A
SARS-CoV-2-RBD-L455RA475R-AVI	This study	N/A
SARS-CoV-2-RBD-L455RG496R-AVI	This study	N/A
SARS-CoV-2-RBD-L455RA475RG502R-AVI	This study	N/A
Critical Commercial Assays		
Turbo293 Transfection Kit	ThermoFisher Scientific Inc.	Cat# A14525
BirA biotin-protein ligase bulk reaction kit	Avidity	BirA500
Deposited Data		
Cryo-EM map: SARS-CoV-2 S2P C1 symmetry	EMDB	EMDB: EMD-22162
Cryo-EM structure: SARS-CoV-2 S2P C1 symmetry	PDB	PDB: 6XF6
Cryo-EM map: SARS-CoV-2 S2P C3 symmetry	EMDB	EMDB: EMD-22161
Cryo-EM structure: SARS-CoV-2 S2P C3 symmetry	PDB	PDB: 6XF5
Experimental Models: Cell Lines		
Expi293F cells	ThermoFisher Scientific Inc	Cat# A14527
FreeStyle 293-F cells	ThermoFisher Scientific Inc	Cat# R79007
Recombinant DNA		
pVRC8400 vector	https://www.addgene.org	Cat# 63160
pVRC8400-CR3022	Yuan et al., 2020	N/A
pVRC8400-S652-109	This study	N/A
pVRC8400-S652-112	This study	N/A
pVRC8400-S652-118	This study	N/A
pVRC8400-SARS-CoV-2-S2P-AVI	This study https://www.addgene.org	Cat# 160474
pVRC8400-SARS-CoV-2-NTD-AVI	This study https://www.addgene.org	Cat# 160475
pVRC8400-SARS-CoV-2-RBD-AVI	This study https://www.addgene.org	Cat# 160476

(Continued on next page)

REAGENT or RESOURCE	SOURCE	IDENTIFIER
pVRC8400-SARS-CoV-2-RBD-SD1-AVI	This study https://www.addgene.org	Cat# 160477
pVRC8400-SARS-CoV-2-RBD-L455RA475R-AVI	This study https://www.addgene.org	Cat# 160478
pVRC8400-SARS-CoV-2-RBD-L455RG496R-AVI	This study https://www.addgene.org	Cat# 160479
pVRC8400-SARS-CoV-2-RBD-L455RA475RG502R-AVI	This study https://www.addgene.org	Cat# 160480
Software and Algorithms		
GraphPad Prism Software	GraphPad Prism Software, Inc.	N/A
Scrubber 2.0	BioLogic Software	http://www.biologic.com.au/scrubber.html
The PyMol Molecular Graphics System, v1.8.6	Schrödinger, LLC	https://pymol.org/2/
BLI Acquisition & Analysis Software	ForteBio	https://www.fortebio.com/products/octet-systems-software
Leginon	Suloway et al., 2005	https://sbgrid.org/software/titles/legion
The PEP-Fold server	Shen et al., 2014 ; Thévenet et al., 2012	https://bioserv.rpbs.univ-paris-diderot.fr/services/PEP-FOLD/
GCTF	Zhang, 2016	https://www.mrc-lmb.cam.ac.uk/kzhang/Gctf/
CTFFind4	Rohou and Grigorieff, 2015	http://grigoriefflab.janelia.org/ctffind4
Dog Picker	Voss et al., 2009	https://omictools.com/dog-picker-tool
RELION	Scheres, 2012	https://www3.mrc-lmb.cam.ac.uk/relion/index.php/Main_Page
cryoSPARC	Punjani et al., 2017	https://cryosparc.com
EMRinger	Barad et al., 2015	http://emringer.com/
Phenix	Adams et al., 2004	https://sbgrid.org/software/
Coot	Emsley and Cowtan, 2004	https://sbgrid.org/software/
UCSF Chimera	Pettersen et al., 2004	https://www.cgl.ucsf.edu/chimera/

RESOURCE AVAILABILITY

Lead Contact

Further information and requests for resources and reagents should be directed to and will be fulfilled by Peter D. Kwong (pdkwong@nih.gov).

Materials Availability

Plasmids for the SARS-CoV-2 probes with AVI tag generated in this study have been deposited with Addgene (www.addgene.org) with accession numbers: 160474-160480.

Data and Code Availability

Cryo-EM maps of the biotinylated SARS-CoV-2 S2P have been deposited to the EMDB with accession codes EMD-22161 (RBDs down) and EMD-22162 (1 RBD up), and fitted coordinates have been deposited to the PDB with accession codes 6XF5 and 6XF6, respectively.

EXPERIMENTAL MODEL AND SUBJECT DETAILS

Patient samples

Peripheral blood mononuclear cells (PBMCs) for B cell sorting were obtained from a convalescent SARS-CoV-2 patient (collected 75 days post symptom onset under an IRB approved clinical trial protocol, VRC 200 – [ClinicalTrials.gov](https://clinicaltrials.gov) Identifier: NCT00067054) and a healthy control donor from the NIH blood bank pre-SARS-CoV-2 pandemic.

PBMCs for experimental sorting of natively paired antibody heavy:light yeast display libraries were obtained from 2 participants enrolled in the COVID-19 Cohort Study at Columbia University Irving Medical Center. Participants were both men in their 50's,

hospitalized for severe respiratory decompensation requiring mechanical ventilation after confirmed SARS-CoV-2 infection. Specimens were obtained at 25 days (1605) and 32 days (NYP01) after symptom onset. Patient samples were collected after obtaining informed consent and appropriate Institutional Review Board approval (IRB#AAAS9517).

Cell lines

Expi293F and FreeStyle 293-F cells were purchased from Thermo Fisher Scientific. The cells were used directly from the commercial sources following manufacturer suggestions as described in detail below.

METHOD DETAILS

Construction of expression plasmids for SARS-CoV-2 probes

DNA sequences coding for the SARS-CoV-2 spike or its domains were cloned into a pVRC8400-based expression vector by Genelmmune. The gene of interest was placed after the DNA sequence encoding a N terminus single chain human Fc with knob-in-hole mutations, a “GGSGGGGSGG” linker and an HRV3C protease cleavage site for purification with protein A column and on-column cleavage. DNA sequence encoding a C terminus “GGGLVPQQSG” linker named 10InQQ and an AVI tag was placed after the gene of interest for biotinylation (Table S1).

For the scFc-SARS-CoV-2 S2P-AVI construct, the cloned insertion included the spike protein residues 14 to 1208 with GSAS replacing the RRAR at the S1/S2 cleavage site and K986P and V987P stabilization mutations, a GSG linker and the T4-phage fibrin trimerization domain (foldon) as described by Wrapp et al. (2020b). For the scFc-SARS-CoV-2 NTD-AVI construct, spike gene encoding residues 14-305 was cloned. For the scFc-SARS-CoV-2 RBD-AVI construct, spike gene encoding residues 329-526 was cloned. For the scFc-SARS-CoV-2 RBD-SD1-AVI construct, spike gene encoding residues 319-591 was cloned. The constructs comprising specific mutations for knocking out ACE2 interaction with RBD were made by site directed mutagenesis in the scFc-SARS-CoV-2 RBD-AVI plasmid, either in double Arg substitutions at L455 and A475 (L455RA475R), or at L455 and G496 (L455RG496R), or in triple Arg substitutions at L455, A475, and G502 (L455RA475RG502R). A model of the 10InQQ linker and AVI tag was obtained on the PEP-FOLD server (Shen et al., 2014; Thévenet et al., 2012) to show the location of this C-terminal addition in Figure S1.

Expression and preparation of SARS-CoV-2 probes

Single chain Fc tagged SARS-CoV-2 probes were produced by transient transfection of 293 Freestyle cells as previously described (Wrapp et al., 2020b). One liter of cells was transfected with 1 mg of SARS-CoV-2 probe plasmid, pre-mixed with 3 mL of Turbo293 transfection reagent. The cells were allowed to grow for 6 days at 120 rpm, 37°C, and 9% CO₂, after which the supernatant was harvested by centrifugation and filtered. The cleared supernatant was incubated with 5ml of PBS-equilibrated Protein A resin for two hours, after which the resin was then collected and washed with PBS. The captured SARS-CoV-2 probe was then concurrently biotinylated with 10–80 μg BirA enzyme (~2.5 μg per 10 nmol AVI substrate) and 100 μM biotin, as well as cleaved from the Fc purification tag with 200 μg of HRV3C, which was prepared as described (Antonioni et al., 2017), in a reaction mixture containing 10 mM Tris pH 8.0, 50 μM bicine, 10 mM ATP, 10 mM Mg(OAc)₂. For RBD and NTD domains, addition of 100 μM DTT in the reaction may facilitate the cleavage but it is optional. After incubation at 4°C overnight, the cleaved protein was collected, concentrated and applied to a Superdex 200 16/60 gel filtration column equilibrated with PBS. Peak fractions were pooled and concentrated to 1 mg/ml.

Expression and preparation of the ACE2 receptor

The human ACE2 (1-620aa) expression plasmid was constructed by placing an HRV3C cleavage site, a monomeric Fc tag and an 8xHisTag at the 3' end of the ACE2 gene. After transient transfection of 293F cells, the cell culture supernatant was harvested 4 days post transfection and loaded onto a Protein A affinity column. The Fc-tagged protein was eluted with IgG elution buffer and then dialyzed against PBS before overnight HRV3C digestion at 4°C. Cleaved protein was passed over a protein A column to remove the Fc tag. ACE2 from the protein A column flow through was further purified with a Superdex 200 16/60 column in 5 mM HEPES, pH7.5 and 150 mM NaCl.

Expression and preparation of antibodies

DNA sequences of antibody heavy and light chain variable regions of antibody CR3022 (Yuan et al., 2020) and of donor S652 antibodies, S652-109, S652-112, and S652-118, and of SARS-CoV-2 antibodies B38 (Wu et al., 2020), 2-4, 4-8, and 2-51 (Liu et al., 2020a) were synthesized and subcloned into the pVRC8400 vector, as described previously (Wu et al., 2011). Antibody expression was carried out by co-transfection of both heavy and light chain plasmids in Expi293F cells (Thermo Fisher) using Turbo293 transfection reagent (Speed BioSystems). On day 6 post transfection, the culture supernatant was harvested and loaded on a protein A column. After washing with PBS for 3 column volumes, IgG was eluted with an IgG elution buffer (Pierce) and immediately neutralized by addition of one tenth volume of 1M Tris-HCl pH 8.0.

Bio-Layer Interferometry

A FortéBio Octet HTX instrument (FortéBio) was used to analyze biotinylation level, antigenicity, and receptor recognition of the molecular probes. Assays were performed at 30°C in tilted black 384-well plates (Geiger Bio-One) in PBS + 0.02% Tween20, 0.1% BSA,

0.05% sodium azide with agitation set to 1,000 rpm. Biotinylated SARS-CoV-2 spike (80 $\mu\text{g/ml}$), NTD (40 $\mu\text{g/ml}$), RBD (5 $\mu\text{g/ml}$), RBD-SD1 (5 $\mu\text{g/ml}$), RBD-L455RA475R (5 $\mu\text{g/ml}$), RBD-L455RG496R (80 $\mu\text{g/ml}$), RBD-L455RA475RG502R (15 $\mu\text{g/ml}$) and HIV Env (20 $\mu\text{g/ml}$) were loaded on to streptavidin biosensors for 150 s. Binding to biotinylated probes was measured by dipping immobilized probes into solutions of receptors and antibodies at 500 nM for 180 s. Receptor and antibody binding were assessed in triplicate. Parallel correction to subtract systematic baseline drift was carried out by subtracting the measurements recorded for a loaded sensor dipped into buffer only control well. The reference corrected response values are reported as averages of maximum signal during the association step.

Surface plasmon resonance

SPR binding experiments were performed using a Biacore T200 biosensor, equipped with either a Series S SA chip for the Fab binding assays, or a Series S CM4 chip immobilized with NeutrAvidin, for the ACE2 binding assays. All measurements were performed at 25°C in a running buffer of 10 mM HEPES pH 7.4, 150 mM NaCl, and 0.05% (v/v) Tween-20.

Biotinylated spike, RBD, and NTD were captured over independent flow cells at 1000–1100 RU, 300–500 RU and 260 RU, respectively. ACE2-analyte samples were prepared in running buffer at a concentration range of 300–1.2 nM using a three-fold dilution series. Binding over the spike and RBD or NTD surfaces as well as over a neutravidin reference surface was tested for 180 s followed by a 300 s dissociation phase at 50 $\mu\text{L/min}$. Blank buffer cycles were performed throughout the experiment by injecting running buffer instead of ACE2 to subtract systematic noise from the binding signal. The data was processed and fit to 1:1 binding model using Scrubber 2.0 (BioLogic Software).

To avoid the need for surface regeneration that arises with the low off-rate Fabs, we used single-cycle kinetics for the Fab binding experiments. Each Fab was tested at analyte concentrations 180–6.66 nM prepared in running buffer using a three-fold dilution series. Binding over the spike or RBD surface or the NTD surface for S652–118, was monitored for 120 s, followed by a dissociation phase of 120 s–900 s depending on the interaction. Four blank buffer single cycles were performed by injecting running buffer instead of Fab to remove systematic noise from the binding signal. The data was processed and fit to 1:1 single cycle model using the Scrubber 2.0 (BioLogic Software).

Negative-stain electron microscopy

Purified SARS-CoV-2 S samples were diluted to approximately 0.02 mg/ml with a buffer containing 10 mM HEPES, pH 7, and 150 mM NaCl. A 4.7- μL drop of the diluted sample was applied to a glow-discharged carbon-coated copper grid. The grid was washed with the same buffer, and adsorbed protein molecules were negatively stained with 0.75% uranyl formate. Micrographs were collected at a nominal magnification of 100,000 \times (pixel size: 0.22 nm) using SerialEM (Mastrorade, 2005) on an FEI Tecnai T20 electron microscope operated at 200 kV and equipped with an Eagle CCD camera. Particles were picked automatically using in-house written software (Y.T., unpublished). Reference-free 2D classification was performed with Relion 1.4 (Scheres, 2012).

Cryo-EM data collection and processing

Biotinylated SARS-CoV-2 spike probe was diluted to a final trimer concentration of 0.33 mg/mL in PBS, pH 7.4. The sample (2 μL) was applied to a glow-discharged carbon-coated copper grid (CF 1.2/1.3) and vitrified using a Vitrobot Mark IV with a wait time of 30 s and a blot time of 3 s.

Data were collected using the Leginon software (Suloway et al., 2005) installed on a Titan Krios electron microscope operating at 300 kV, equipped with a Gatan K3–BioQuantum direct detection device. The total dose was fractionated for 3 s over 60 raw frames. Motion correction, CTF estimation, particle picking and extraction, 2D classification, *ab initio* model generation, 3D refinements and local resolution estimation were carried out in cryoSPARC 2.14 (Punjani et al., 2017). The 3D reconstructions were performed using C3 symmetry for the RBDs down map while C1 symmetry was applied for the 1 RBD up map. Local refinement (beta) with C1 symmetry was performed on the RBDs down map using a mask focused on the C-terminal helices, which included the bottom of the S2 subunit spanning from residue 1070 to the C terminus. The overall resolution was 3.45 Å for the RBDs down map, 4.00 Å for the 1 RBD up map, and 4.28 Å for the RBDs down local refinement map, confirmed by providing the half maps to Resolve Cryo EM in Phenix (Adams et al., 2004).

Cryo-EM model fitting

The coordinates of SARS CoV-2 spike ectodomain structures, PDB entries 6VXX and 6VYB (Walls et al., 2020), were employed as initial models for fitting the cryo-EM map of the RBDs down and the 1 RBD up conformation respectively. In both structures, the RBDs in the “down” position were modeled using the crystallographic structure of RBD in complex with CR3022 Fab (PDB entry 6W41) (Yuan et al., 2020) as a template. For the RBD in the “up” position the map quality did not allow visualization of most side chains which were then modeled as poly-Ala, consistent with what observed for 6VYB (Walls et al., 2020). Manual and automated model building were iteratively performed using Coot (Emsley and Cowtan, 2004) and real space refinement in Phenix respectively, in order to accurately fit the coordinates to the electron density map. Half maps were provided to Resolve Cryo EM tool in Phenix to support manual model building. EMRinger (Barad et al., 2015) and Molprobit (Davis et al., 2004) were used to validate geometry and check structure quality at each iteration step. UCSF Chimera (Pettersen et al., 2004) was used for map-fitting cross correlation calculation (Fit-in-Map tool) and for figure preparation.

Probe conjugation

Biotinylated SARS-CoV-2 spike probes were conjugated using either allophycocyanin (APC)-, phycoerythrin (PE)-, BV421-, BV711-, or BV786-labeled streptavidin. Reactions were prepared at a 4:1 molecular ratio of protein to streptavidin, with every monomer labeled. Labeled streptavidin was added in $\frac{1}{5}$ increments, with incubations at 4°C (rotating) for 20 minutes in between each addition.

Monoclonal yeast display analysis

Yeast display analysis using monoclonal yeast were created, expressed and analyzed as previously published (Wang et al., 2018a). Briefly, VH and VL regions of S652-109, S652-112 and S652-118 were codon optimized for yeast expression, synthesized and cloned into pCT-VHVL-K1 or pCT-VHVL-L1 yeast expression vectors (Genscript). Yeast display vectors were linearized and *Saccharomyces cerevisiae* strain AWY101 (MAT α AGA1::GAL1-AGA1::URA3 PDI1::GAPDH-PDI1::LEU2 ura3-52 trp1 leu2 Δ 1 his3 Δ 200 pep4::HIS3 prb1 Δ 1.6R can1 GAL) was transformed. Yeast cells were maintained in YPD medium (20 g/l dextrose, 20 g/l peptone, and 10 g/l yeast extract); after library transformation, yeast cells were maintained in SDCAA medium (20 g/l dextrose, 6.7 g/l yeast nitrogen base, 5 g/l casamino acids, 8.56 g/l NaH₂PO₄·H₂O, and 10.2 g/l Na₂HPO₄·7H₂O). Fab display was induced by incubating yeast in SGDCAA medium (SDCAA with 20 g/l galactose, 2 g/l dextrose). Two days after induction, 1x10⁶ yeast were incubated in staining buffer (phosphate buffered saline + 0.5% BSA + 2mM EDTA) containing anti-Flag fluorescein isothiocyanate antibody (2 μ g/mL; clone M2, Sigma-Aldrich) and the probes for 30 minutes on ice prior to washing 2 times in ice cold staining buffer. Fab expressing yeast (FLAG+) were analyzed for their capacity to bind to the indicated probes using a FACS Aria II (BD Biosciences). For single probe stain experiments yeast were incubated with 4 ng/ μ l of S2P (APC) for mAb S652-109 and 2 ng/ μ l for mAbs S652-112 and S652-118, 2 ng/ μ l of RBD-SD1 (BV421) or 2 ng/ μ l of RBD-L455RA475RG520R (BV786). Dual stain experiments used 4 ng/ μ l of S2P (APC), 2 ng/ μ l of RBD-SD1 (BV421) or 2 ng/ μ l of RBD-L455RA475RG520R (BV786).

Experimental sorting of natively paired antibody heavy:light yeast display libraries

Non-B cells were depleted (EasySep Human B cell enrichment kit w/o CD43 Depletion, STEMCELL Technologies, Vancouver, Canada) and CD27⁺ antigen-experienced B cells were isolated by positive magnetic bead separation (CD27 Human Microbeads, Miltenyi Biotec, Auburn, CA, respectively) (Lagerman et al., 2019). Antigen-experienced B cells were stimulated *in vitro* for five days to enhance antibody gene transcription in the presence of Iscove's Modified Dulbecco's Medium (IMDM) (ThermoFisher Scientific, NY, USA) supplemented with 10% FBS, 1 \times GlutaMAX, 1 \times non-essential amino acids, 1 \times sodium pyruvate and 1 \times penicillin/streptomycin (Life Technologies, Carlsbad, California, USA) along with 100 units/mL IL-2 and 50 ng/mL IL-21 (PeproTech, Rocky Hill, NJ, USA), and were co-cultured with irradiated 3T3-CD40L fibroblast cells that secrete CD40L to aid B cell expansion. Stimulated B cells were emulsified in the presence of lysis buffer and magnetic beads for mRNA capture as previously described (DeKosky et al., 2015). Magnetic beads were collected and re-emulsified in an overlap-extension RT-PCR emulsion (SuperScript III One-Step RT-PCR System with Platinum Taq DNA Polymerase, ThermoFisher Scientific, NY, USA) to generate linked VH:VL amplicons (DeKosky et al., 2013, 2015; McDaniel et al., 2016; Wang et al., 2018a). cDNA was extracted and a nested PCR was performed (Kapa HiFi HotStart PCR Kit, Kapa Biosystems) to generate ~850-bp VH:VL products for library cloning into yeast display. 100 ng of natively paired cDNA was amplified with primers containing NotI and Ascl restriction sites for cloning into bidirectional yeast display plasmids (Wang et al., 2018a). Libraries were transformed for amplification in *E. coli*, followed by plasmid DNA extraction and subcloning of a galactose-inducible bidirectional promoter. The resulting native Fab display libraries were co-transformed into electrocompetent AWY101 with Ascl/NotI digested pCT vector into yeast cells, and passaged twice before screening (Wang et al., 2018a). Yeast libraries were cultured in SGDCAA medium to induce Fab surface-expression at 20°C and 225 rpm for 36 hours prior to antigen staining. Libraries were stained with an anti-FLAG-FITC monoclonal antibody (clone M2, Sigma-Aldrich, St. Louis, MO), and either 20 nM of fluorescently labeled S2P or 100 nM of fluorescently labeled NTD or RBD probes, respectively, to isolate antigen binding Fabs. Yeast cells that were gated for Fab expression and antigen binding and collected via fluorescence-activated cell sorting (FACS) and cultured for 48 hours. Libraries were re-induced and re-stained for additional rounds of selection and for the analysis of antigen binding after sorting.

PBMC B cell stain

Frozen PBMCs were thawed and immediately stained for viability using the Fixable Aqua Dead Cell Stain Kit (ThermoFisher). The PBMCs were stained with the following human surface markers: IgG (G18-145), IgA (S11-8E10), IgM (G20-127), CD8 (RPA-T8), CD3 (OKT3), CD56 (HCD56), CD14 (M5E2), CD27 (O323), CD19 (J3-119), CD38 (HIT2), and CD20 (2H7), sourced from BD, Biolegend, Beckman, and Miltenyi, as well as SARS-CoV-2 probes (2019 S2P, RBD, RBD-SD-1, RBD ACE2KO, and NTD) in Brilliant Stain Buffer (BD). Samples were collected on a BD FACS-ARIA III and analyzed with FlowJo v10.6.1.

QUANTIFICATION AND STATISTICAL ANALYSIS

The statistical analyses for the BLI assessment of probe-antibody binding were performed using GraphPad Prism. The SPR data were processed and fit to a 1:1 binding model using Scrubber 2.0 (BioLogic Software).